Precambrian Research 174 (2009) 35–52

Contents lists available at ScienceDirect

Precambrian Research

journal homepage: www.elsevier.com/locate/precamres

Palaeomagnetism and magnetic anisotropy of late Neoproterozoic strata, South Australia: Implications for the palaeolatitude of late Cryogenian glaciation, cap carbonate and the Ediacaran System

Phillip W. Schmidt[a,*], George E. Williams[b], Michael O. McWilliams[c]

[a] CSIRO Exploration and Mining, PO Box 136, North Ryde, NSW 1670, Australia
[b] Discipline of Geology and Geophysics, School of Earth and Environmental Sciences, University of Adelaide, SA 5005, Australia
[c] CSIRO Exploration and Mining, PO Box 883, Kenmore, Qld 4069, Australia

ARTICLE INFO

Article history:
Received 25 November 2008
Received in revised form 17 May 2009
Accepted 1 June 2009

Keywords:
South Australia
Neoproterozoic
Glaciation
Elatina Formation
Nuccaleena Formation
Palaeomagnetism

ABSTRACT

The Ediacaran Global Stratotype Section and Point (GSSP) is defined near the base of the Nuccaleena Formation, the "cap carbonate" overlying the terminal Cryogenian glaciogenic Elatina Formation at a basin-wide sequence boundary in the Adelaide Geosyncline, South Australia. Previous palaeomagnetic data for 205 specimens from the Elatina Formation yielded a structurally corrected mean declination $D = 208.3^\circ$ and inclination $I = -12.9^\circ$ ($\alpha_{95} = 4.2^\circ$), palaeolatitude $\lambda = 6.5 \pm 2.2^\circ$ and pole position at latitude $\lambda_p = 47.3^\circ$S, longitude $\varphi_p = 359.3^\circ$E (dp = 2.1° and dm = 4.2°). New palaeomagnetic data for 141 specimens from the Nuccaleena Formation yield a structurally corrected mean direction of $D = 208.3^\circ$, $I = -34.9^\circ$ ($\alpha_{95} = 3.4^\circ$), $\lambda = 19.2 + 2.3/-2.2^\circ$ and pole position at $\lambda_p = 32.3^\circ$S, $\varphi_p = 350.8^\circ$E (dp = 2.2° and dm = 3.9°). There is a substantial difference in inclination between the Elatina and Nuccaleena formations, despite their juxtaposition. Positive fold tests for both formations seem to rule out remagnetisation of one or both formations. Fold tests on tepee-like structures in the Nuccaleena Formation accord with the magnetisation having been acquired at or near the time the structures formed during early diagenesis. Magnetisation therefore variably lags deposition, causing the three identified magnetostratigraphic horizons to appear highly bedding-transgressive; whereas local correlations may seem satisfactory, regional correlations are not. Nevertheless, the number and duration of polarity chrons at various localities appear valid, implying that the Nuccaleena Formation accumulated over an interval of $>10^5$ years.

The question of compaction-related inclination shallowing was addressed by examining the anisotropy of remanence using a superconducting 12 T magnet. The effective flattening factors f determined were: Nuccaleena dolostones, $N = 4$, $f = 0.98 \pm 0.02$; Elatina tidal rhythmites, $N = 6$, $f = 0.97 \pm 0.01$; Elatina arenites, $N = 9$, $f = 0.92 \pm 0.02$. The mean Elatina inclination is corrected to -14.0° (palaeolatitude of 7.1°) and the mean Nuccaleena inclination to -35.4° (palaeolatitude of 19.6°). Inclination shallowing also was investigated using the Elongation–Inclination method. The distributions of directions for the Elatina were somewhat skewed with respect to bedding, possibly invalidating use of this method. Nevertheless, for the Elatina the method yields an inclination of -19° (palaeolatitude of 10°). For the Nuccaleena, the corrected inclination is -41.9° (palaeolatitude of 24°). These corrections do not materially alter the near-equatorial palaeolatitude for the Elatina Formation, which is supported by data for other Neoproterozoic strata in southern Australia. However, the substantial increase in palaeolatitude between the late Cryogenian and the early Ediacaran is maintained.

The sequence boundary below the Nuccaleena Formation is a disconformity to low-angle unconformity that in places cuts deeply into the ~1500 m thick, late Cryogenian glaciogenic succession, and may represent a significant time gap marked by rapid polar wander. Such a hiatus may be an important factor in the juxtaposition of glacial deposits and cap carbonates.

1. Introduction

The late Cryogenian and Ediacaran constitute an enigmatic interval in the Earth's history, with near-equatorial glaciations close to sea level, followed by apparent warm-water carbonates and later by the widespread appearance of multicellular animal life. In the

* Corresponding author. Fax: +61 2 9490 8960.
E-mail address: phil.schmidt@csiro.au (P.W. Schmidt).

0301-9268/$ – see front matter.
doi:10.1016/j.precamres.2009.06.002

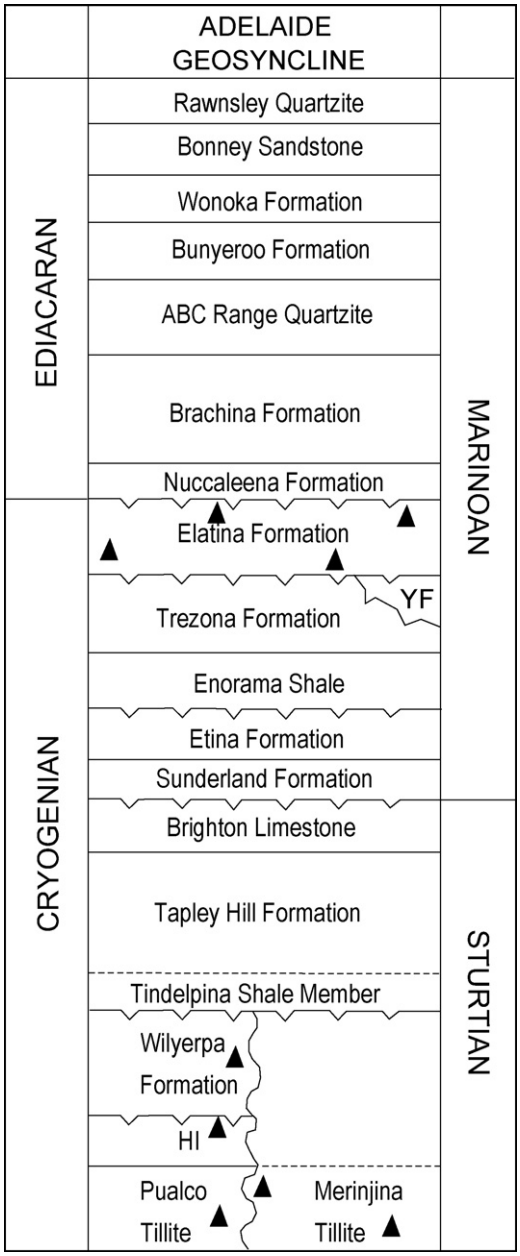

Fig. 1. Generalised stratigraphy of Cryogenian and Ediacaran strata in the Adelaide Geosyncline (Central Flinders Zone), South Australia. Glaciogenic formations are shown with solid triangles. YF, Yaltipena Formation; HI, Holowilena Ironstone. Adapted from Preiss et al. (1998) and Williams et al. (2008).

Neoproterozoic succession of South Australia (Fig. 1), the late Cryogenian glaciogenic Elatina Formation is overlain disconformably to unconformably by the Ediacaran "cap carbonate" Nuccaleena Formation (Fig. 2e), with the Nuccaleena–Elatina contact being interpreted as a basin-wide sequence boundary (Preiss, 2000; Williams et al., 2008, in press). The recently established Ediacaran System and Period (Knoll et al., 2004, 2006) has its Global Stratotype Section and Point (GSSP) purportedly placed at the base of the Nuccaleena Formation in the central Flinders Ranges. As discussed by Williams et al. (2008, in press), the GSSP appears to be placed within a conformable succession below prominent dolostone beds of the Nuccaleena Formation and above a 0.2–0.3 m thick bed of pale red sandstone that disconformably overlies the Elatina Formation. This sandstone may be a local development of the basal Ediacaran Seacliff Sandstone, which interfingers with the Nuccaleena Formation in the southern Adelaide Geosyncline (Forbes and Preiss, 1987).

It is now widely accepted that the terminal Cryogenian Elatina glaciation in South Australia occurred close to sea level in near-equatorial palaeolatitudes. Most palaeomagnetic samples from the Elatina Formation were Type A red beds (Turner, 1980) of fine-, medium- and coarse-grained sandstone containing ultrafine hematite. Mudstones and muddy diamictites were not sampled. Palaeomagnetic low inclinations characterised samples from the contrasting tectonic settings of the Adelaide Geosyncline, where deep burial and folding occurred, and from horizontal strata on the adjacent cratonic Stuart Shelf where depths of burial were much less (Schmidt and Williams, 1995). The early timing of magnetic remanence in the Elatina Formation is confirmed by positive soft-sediment fold tests at high levels of confidence for slump folds in tidal rhythmites that contain silt-sized detrital hematite grains (Schmidt et al., 1991; Schmidt and Williams, 1995; Williams, 1996; Williams et al., 2008, in press).

The observation of mixed polarities for some Elatina specimens implies chemical remanent magnetisation (CRM) acquired over a protracted interval of time, and hence it is appropriate to use specimen directions, rather than site directions, to provide an overall formation mean direction (Schmidt and Williams, 1995). Combined data for the Elatina Formation (Schmidt and Williams, 1995; Sohl et al., 1999, Geological Society of America Data Repository item NNN) for 205 specimens yielded a structurally corrected mean declination $D = 208.3^\circ$ and mean inclination $I = -12.9^\circ$ ($\alpha_{95} = 4.2^\circ$), and a pole position at latitude $\lambda_p = 47.3^\circ$S, longitude $\varphi_p = 359.3^\circ$E with confidence semi-axes $dp = 2.1^\circ$ and $dm = 4.2^\circ$. A palaeolatitude $\lambda = 6.5 \pm 2.2^\circ$ is indicated by applying the dipole equation:

$$\tan I = 2 \tan \lambda \quad (1)$$

The apparent palaeoclimatic contradiction of low-palaeolatitude glacial deposits overlain by presumed warm-water carbonates has long been recognised (e.g. Williams, 1979). The implied rapid climate change has given rise to conflicting interpretations of the nature of low-palaeolatitude glaciations and glacial termination (Jenkins et al., 2004). In the "Snowball Earth" scenario of Hoffman and Schrag (2002), the cap carbonates, which follow many Neoproterozoic glaciogenic successions, formed during rapid deglaciation (<10^4 years) accompanying sea-level rise under extreme greenhouse regimes. In apparent conflict, magnetostratigraphic studies of Neoproterozoic cap carbonates from Australia, Africa and South America record multiple polarity transitions which suggest that deposition of the cap carbonates lasted 10^5 to 10^6 years (Li, 2000; Trindade et al., 2003; Kilner et al., 2005; Raub and Evans, 2005).

Here we investigate the palaeomagnetism of the Nuccaleena Formation with respect to the growth of diagenetic tepee-like structures (Gammon et al., 2005) and regional folding, compare these results to findings for the Elatina Formation and other Neoproterozoic strata in southern Australia, and study the anisotropies of magnetic susceptibility and remanence of the Elatina and Nuccaleena formations as an aid to elucidating the process of remanence acquisition. We also examine the magnetostratigraphy of the Nuccaleena Formation to place time constraints on the interval of cap carbonate deposition.

2. Previous palaeomagnetic data for Neoproterozoic cap carbonates

Sohl et al. (1999) sampled the pink to pale red dolostones from the Nuccaleena Formation at three sections (Bennett Spring, Trezona Bore, and Warcowie) in the Central Flinders Ranges, South Australia. They found poorly defined components and scattered directions, concluding that the carbonates carry unstable magneti-

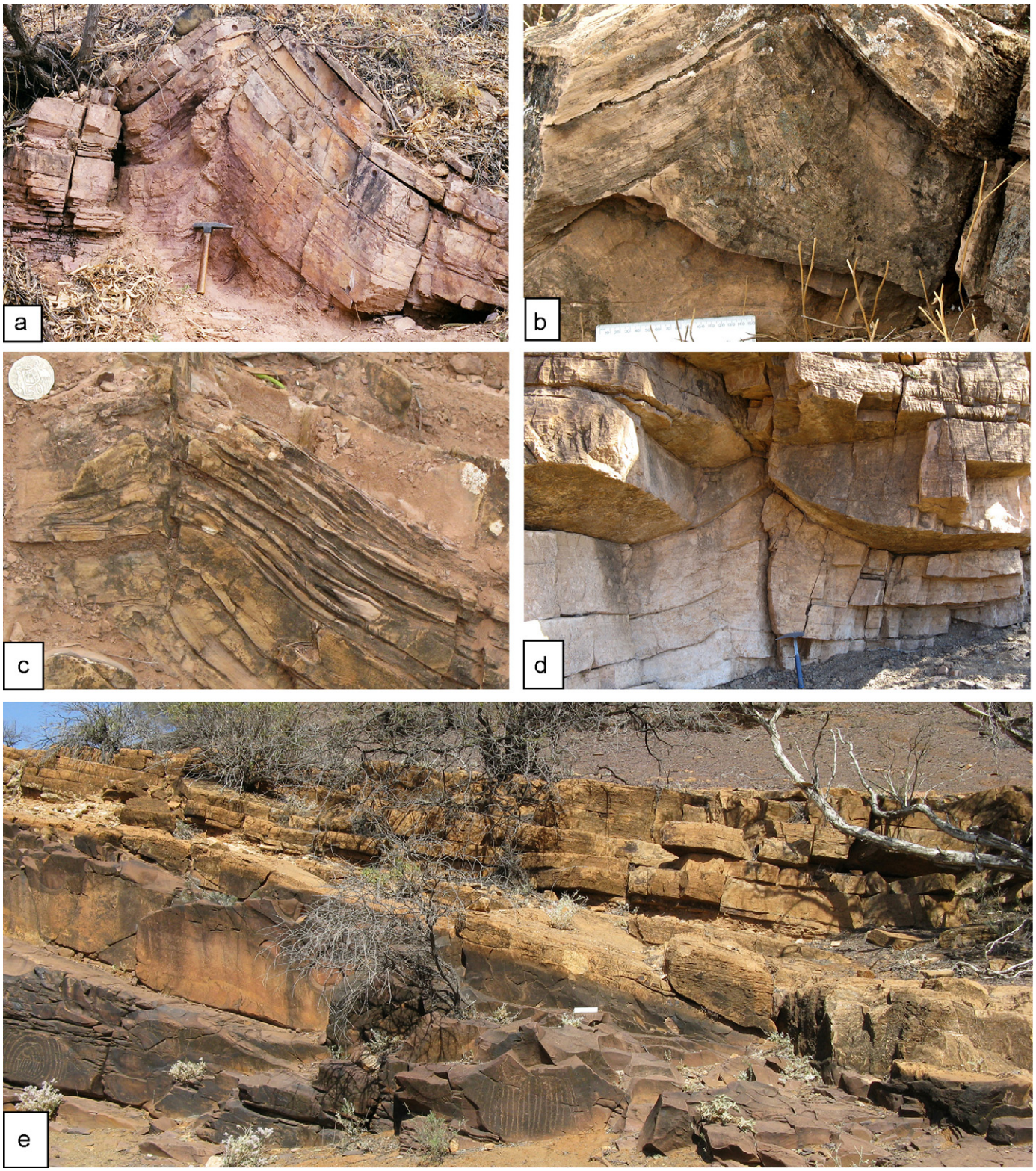

Fig. 2. (a–d) Tepee-like structures in dolostone of the Nuccaleena Formation, Flinders Ranges, South Australia. (a) Tepee-like anticline with axial-plane fault, at site NF01 near the top of the Nuccaleena Formation in Enorama Creek. Hammer 35 cm long. (b) Cuspate tepee-like structure with internal disruption of strata and small voids filled with sparry carbonate, Enorama Creek. Scale 15 cm. (c) Small tepee-like structure at site NF08 in Angorichina Creek. Coin 3 cm in diameter. (d) Cuspate tepee-like structure draped by beds that thin over the crest, in tributary of Mount Chambers Creek. Hammer 33 cm long. Structures at sites NF04 and NF07 have this form. (e) Viewer looking west to dolostone beds of the Nuccaleena Formation unconformably onlapping an irregular surface developed on the Elatina Formation, in tributary of Mount Chambers Creek. Section 4 m thick.

sations unsuitable for use in palaeomagnetic studies. Since then, however, sequential magnetic reversals, geomagnetic polarity transitions or dual polarities have been found in Neoproterozoic cap carbonates on other continents, and also in the Nuccaleena Formation.

The pink cap carbonate of the Neoproterozoic Walsh Tillite (Corkeron, 2007, 2008) in the Kimberley region of Western Australia was palaeomagnetically studied by Li (2000). The stratigraphic position of the Walsh Tillite within the Neoproterozoic succession is uncertain, although Li (2000) correlated it with the Sturtian glacial deposits in South Australia. He identified two prominent components, each of dual polarity. The less stable component with unblocking temperatures $T_{ub} < 500\,^{\circ}C$ is parallel to the present local geomagnetic field. Thermal and alternating field (AF) demagnetisation spectra indicated it is carried by fine-grained hematite and goethite and is probably a combination of viscous remanence and weathering-related CRM. The more stable component with T_{ub} from ~500 °C to ~680 °C is directed southeasterly and moderately steeply upward (structurally corrected $D = 148.6^{\circ}$, $I = -63.3^{\circ}$). Because the maximum observed T_{ub} was close to the Curie point of hematite and the dolostone is of a pinkish red hue, Li (2000) surmised that this component is carried entirely by hematite. Further, it was argued that the presence of several stability criteria suggests that this high temperature remanence may be primary in origin: (1) a positive tectonic fold test; (2) the lack of any identified pervasive remagnetising event in the region (notwithstanding the recognised effects of weathering); and (3) petrographic evidence that the hematite is of depositional origin. Although the stratigraphic levels of sites were not reported, only 4 of the 27 samples that yielded high temperature components possessed positive inclinations, suggesting that the Walsh cap carbonate is predominantly of reverse polarity.

The Puga cap carbonate near Mirassol d'Oeste in Brazil (Amazon craton) has been studied palaeomagnetically by Trindade et al. (2003) and Font et al. (2005). Two remanence components were identified: one for carbonate from the deformed Paraguay Belt fails a fold test and is thought to be associated with the early Cambrian Brasiliano orogeny, and another for rocks from the craton with shallow inclinations of dual polarity. Although no fold test is reported for the cratonic sites, the dual polarity directions pass the McFadden and McElhinny (1990) reversal test with 99% confidence. The directions are steeper, and have declinations much closer to true north than the present local geomagnetic field, and are somewhat steeper than the present dipole field. Nevertheless, the directions may record late Tertiary remagnetisation.

Font et al. (2005) carried out an intensive rock magnetic and SEM study to identify and characterise the magnetic carriers in an effort to clarify the origin of the Puga cap carbonate remanence. They showed that detrital specular hematite is the main carrier with rock magnetic properties that are incompatible with remagnetised carbonates, supporting the interpretation of early remanence acquisition. Five polarity chrons were identified in the lower 20 m of the Puga cap carbonate, leading Trindade et al. (2003, p. 445) to conclude that the deposition of the Puga cap carbonate would have spanned "hundreds of thousands of years at least".

The Hadash Formation is a cap carbonate unit above the glaciomarine Fiq diamictite of the Huqf Supergroup, Oman. The Huqf Supergroup has been studied palaeomagnetically by Kilner et al. (2005), who identified two components. One component fails a fold test and is not significantly different from the present local geomagnetic field and is therefore interpreted as being of recent origin, possibly due to weathering. The second component has T_{ub} commonly between 400 and 600 °C and passes a fold test, is of dual polarity and with six stratabound transitions, four of which can be correlated across distinct basins. This component is interpreted as the primary magnetisation. The identification of a sharply defined reversal towards the top of the cap carbonate led Kilner et al. (2005, p. 415) to suggest "that deposition of this unit (the cap carbonate) could have taken place over time scales of at least 10^5–10^6 yr".

Raub and Evans (2005) briefly discussed the implications of three polarity chrons they identified within the Nuccaleena Formation, which suggested to these workers that the cap carbonates were deposited during a time interval of $>10^5$ years. Raub et al. (2007) studied the magnetic properties and mineralogy of the magnetic carriers in the Nuccaleena Formation and showed that detrital hematite is present in association with clay floccules. They observed that magnetite produced during thermal demagnetisation may obscure the recognition of any original magnetite component, and concluded that a direct field test of the Nuccaleena magnetisation component(s) would provide the most reliable evidence for the relative timing of magnetisation acquisition.

3. Tepee-like structures in the Nuccaleena Formation

Tepee-like structures commonly with cuspate crests and amplitudes ranging from a few centimetres up to 1 m are numerous in the microcrystalline (3–30 μm) dolostone units of the Nuccaleena Formation (Plummer, 1978; Lemon and Gostin, 1990; Kennedy, 1996; Gammon et al., 2005). Unlike shallow-water tepees (Kendall et al., 1987), however, the structures lack associated intraclastic breccias and tend to form polygons that are elongate (up to tens of metres long) rather than of regular form.

The tepee-like structures in the Nuccaleena Formation commonly display axial-plane faults and fractures (Fig. 2a and c) and some show internal disruption of beds and voids filled with sparry carbonate (Fig. 2b) (Lavin, 1992; Knoll et al., 2006, their Fig. 6b). Bedding dips attain 70° relative to adjacent undisturbed strata. Some crests are truncated and many structures are draped by subsequent beds that thin or wedge-out over the crests (Fig. 2d) (Lavin, 1992; Kennedy, 1996). According to Gammon et al. (2005), the growth of microcrystalline dolomite in the Nuccaleena Formation caused tepee-like forms and fluid overpressure fracturing in the early diagenetic zone several metres below the sediment–water interface. That many structures formed at or very near the sediment–water interface is indicated by the truncation and draping of crests. Similar tepee-like structures characterised by cores of stromatactis-like cavities occur in the late Cryogenian Doushantuo cap carbonate in south China, and likewise were ascribed to early diagenetic processes (Jiang et al., 2006). The presence of early diagenetic features and internally disrupted beds, together with the microcrystalline textures and steep dips, militate against the tepee-like structures in the Nuccaleena Formation being wave-generated giant ripples (cf. Allen and Hoffman, 2005).

The pink to pale red hue of dolostones of the Nuccaleena Formation results from the presence of ultrafine hematite pigmentation, indicating that these rocks may be suitable palaeomagnetic material. The tepee-like structures represent an opportunity of applying a direct field test to constrain the timing of remanence acquisition of the Nuccaleena Formation relative to early diagenesis. The structures produce steep bedding dips with variable strike orientation, enabling a sampling strategy that incorporates a fold test, modified because the structures commonly have a plunge; the bedding poles and characteristic remanent magnetisation (ChRM) direction must be corrected for plunge before unfolding the residual tepee-like structure.

4. New palaeomagnetic data for the Nuccaleena Formation

4.1. Sampling sites

We collected 142 samples at 12 sites (Fig. 3) in the Nuccaleena Formation. Eight sites provided conventionally grouped samples,

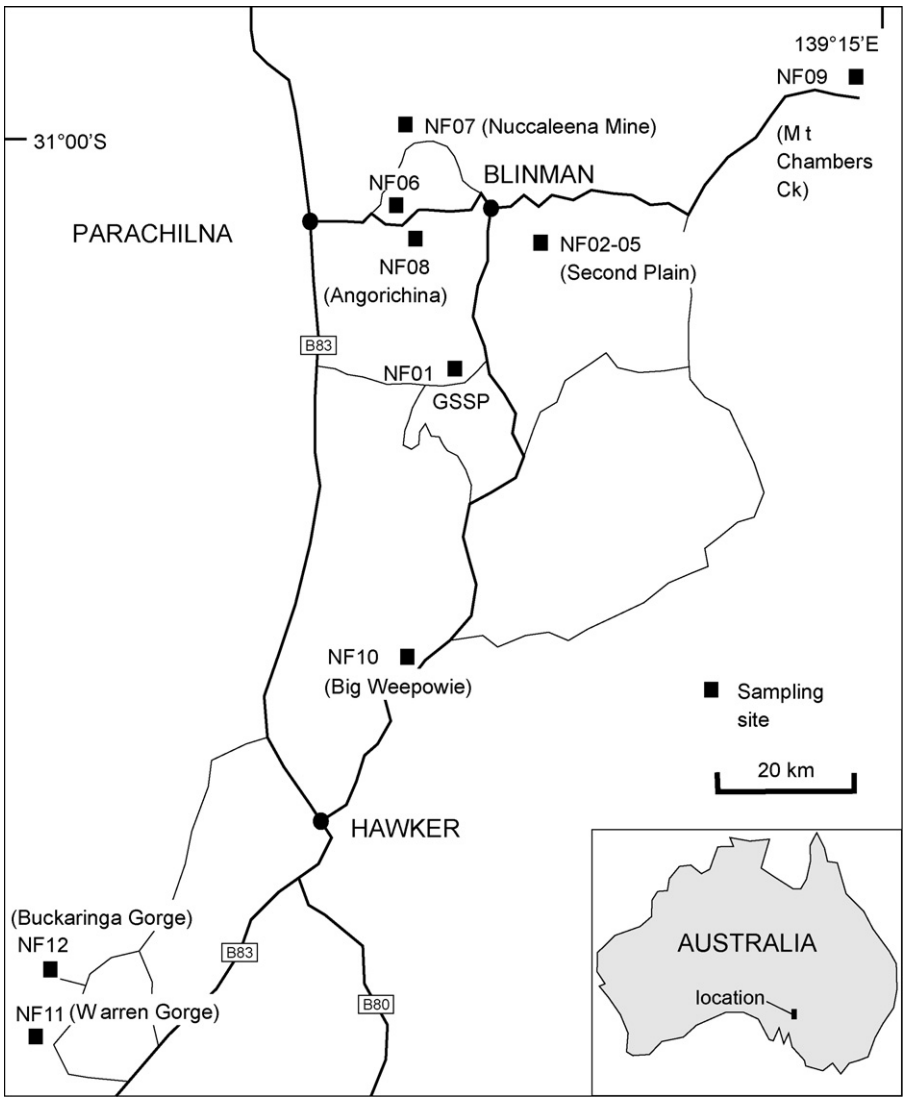

Fig. 3. Map showing palaeomagnetic sampling sites in the Nuccaleena Formation, Flinders Ranges. Site details are given in Appendix A.

whereas four sites were sections through the total thickness of the formation as identified by prominent dolostone beds. Samples comprised dolostone and silty dolostone. Geographic coordinates and bedding attitudes for all sites are given in Appendix A. For the stratigraphic sections at Second Plain (NF02 and NF03), Warren Gorge (NF11) and Buckaringa Gorge (NF12), samples were collected every 10–20 cm. Sites NF01, NF04, NF07 and NF08 included tepee-like structures that required plunge corrections before the observed magnetisation directions were corrected for residual bedding dip. None of the tepee-like structures we sampled occurs at the Elatina–Nuccaleena contact.

4.2. Methods

A portable rock drill was used to take 2.5 cm diameter cores at seven sites/sections, and three to six oriented block samples were collected at each of five sites. Between three and nine specimens were cut from the block samples and at least two specimens per block were processed. Remanent magnetisation was measured using 2G 755R three-axis cryogenic magnetometers at the University of Western Australia and at CSIRO, North Ryde, NSW. The demagnetisers used were in-line 2G 600 series alternating field (AF) demagnetisers and Magnetic Measurements MMTD80 shielded furnaces. All specimens were subjected to 10–15 stepwise thermal demagnetisation steps.

A Sapphire S12B susceptibility instrument was used to measure low field magnetic susceptibility and anisotropy of magnetic susceptibility, and an Oxford PSX120-10 superconducting magnet with a field of 12 T used to impart saturation isothermal remanent magnetisations.

Magnetisation components were isolated using an interactive version of Linefind (Kent et al., 1983), in which linear segments are fitted to data points weighted according to the inverse of their measured variances. The highest temperature to which any particular component remains stable (the highest unblocking temperature observed) was taken as an indication of the Curie temperature of the mineral carrying that component.

4.3. Characteristic magnetisations

Our results are summarised in Table 1 and orthogonal projections of the demagnetisation vectors for representative specimens shown in Fig. 4. As reported by Raub et al. (2007), the dolostone is thermally labile and above 350 °C magnetite was produced from some iron minerals. Siderite commonly is associated with this phenomenon but was not identified here. Although great care

Table 1
Palaeomagnetic summary for the Nuccaleena Formation (mean site $\lambda_s = 31.6°S$, $\varphi_s = 138.8°E$).

Site	N	D_h (°)	I_h (°)	k	α_{95} (°)	D_b (°)	I_b (°)	k	A_{95} (°)
NF01	8	204.8	−41.4	10.7	17.7	193.3	−39.9	23.7	11.6
NF02	19	217.3	−46.7	27.3	6.5	222.2	−32.9	27.3	6.5
NF03	8	200.6	−48.8	13.6	15.6	209.2	−37.0	13.6	15.6
NF04	8	203.7	−44.5	82.1	6.1	210.6	−32.2	82.1	6.1
NF05	3	248.5	−57.8	227	8.2	227.1	−42.8	227	8.2
NF06	6	233.0	−6.0	24.7	13.7	201.8	−27.3	24.7	13.7
NF07	10	252.0	−59.1	5.8	21.9	225.0	−56.4	9.9	16.2
NF08	25	215.1	4.2	14.3	7.9	213.5	−30.6	12.7	8.5
NF09	11	235.9	−41.5	81.0	5.1	215.4	−43.7	81.0	5.1
NF11	43	158.9	−20.7	14.3	6.0	195.2	−29.2	14.3	6.0
Mean	$N = 141$	198.2	−30.9			208.3	−34.9		
		$k = 4.4$	$\alpha_{95} = 6.5°$			$k = 13.1$	$\alpha_{95} = 3.4$		

Structurally corrected pole position: $\lambda_p = 32.3°S$, $\varphi_p = 350.8°E$, dp = 2.2°, dm = 3.9°.
N, number of specimens showing ChRM; α_{95}, half-angle of the 95% confidence cone for the mean direction; D_h and I_h, *in situ* declination and inclination; D_b and I_b, declination and inclination with respect to bedding; k, precision parameter of Fisher (1953) distribution for mean directions; A_{95}, half-angle of the cone of 95% confidence; dp, dm, semi-axes of error ellipse around the pole of probability of 95%.

was taken with shielding, laboratory-induced magnetisation was impossible to prevent in approximately half of the specimens, particularly above 600 °C. The remaining specimens were less problematic but almost all had acquired small but easily measurable laboratory magnetisation after heating to 680 °C but before measurement (see NF01a1, NF01e1 and NF11w1 in Fig. 4a, b and d, where it is evident that the magnetisation vector does not decay directly to the origin). For these specimens, high-temperature components defined by principal component analysis were anchored to the origin.

Notwithstanding the production of magnetite during thermal demagnetisation, the remanent magnetisation of the least affected specimens of the Nuccaleena Formation displayed distributed unblocking temperatures up to 300–400 °C, with little change on further heating until above 660 °C. The remaining remanence was unblocked over a discrete temperature range of 660–680 °C, implying that hematite is the principal magnetic carrier. Although rare, some specimens appear to carry a bipolar component above 660 °C (e.g. NF11m1, Fig. 4f). This magnetisation is further discussed below in terms of duration of remanence acquisition.

ChRM high temperature components were identified in 141 specimens. The low-temperature magnetisation component was directed generally towards the present field and is interpreted as a viscous remanence with no geological significance. In geographic coordinates, the high-temperature components were scattered but fall into two broad groupings to the north and shallowly down or to the south and shallowly up (Fig. 5a). The ChRM directions from tepee-like structures were used according to whether the individual structure displayed directions that appear to be pre-, post- or syn-tepee-formation. That is, if directions appeared to pre-date tepee formation then the fully corrected (deplunged and untilted) directions were used, if the directions appeared to post-date tepee formation then only the regional untilting was applied, and if directions appeared to be syn-tepee-formation then regional untilting was applied to the directions showing least correlation to the tepee-like structure (only site NF07 falls into this last category—details of results from tepee-like structures are discussed below). A fold test is positive with a high degree of confidence. For the 141 directions the Scos1 statistic (McFadden, 1990), which is a measure of correlation between structural orientation and deflection of directions away from the mean direction, decreases from 112 to 11.8 on structural correction. Compared to the 95% and 99% significance points of 13.8 and 19.5, these values indicate a positive fold test with 99% confidence. The results show that the magnetisation was acquired prior to the Delamerian Orogeny at 514–490 Ma (late Early to Late Cambrian; Gradstein et al., 2004), when strata in the Adelaide Geosyncline were deformed (Drexel and Preiss, 1995; Foden et al., 2006).

Directions after structural correction are shown in Fig. 5b. The mean direction for 141 specimens is declination $D = 208.3°$, inclination $I = -34.9°$ ($\alpha_{95} = 3.4°$), indicating a palaeolatitude $\lambda = 19.2 + 2.3/-2.2°$ and a pole position at latitude $\lambda_p = 32.3°S$, longitude $\varphi_p = 350.8°E$, with confidence semi-axes dp = 2.2° and dm = 3.9° (Table 1).

4.4. Results for tepee-like structures

Before conducting fold tests on tepee-like structures, directions and bedding attitudes were corrected for any plunge present. The fold tests are shown in Fig. 6. For site NF01, which is a structure at the GSSP site in Enorama Creek (Fig. 2a), the Scos1 statistic for $N = 8$ decreases from 3.6 to 1.3 and the 95% confidence point is 3.3. This suggests that the magnetisation of the Nuccaleena Formation at the GSSP site pre-dates the formation of this tepee-like structure, because the correlation of directional scatter with structural orientation is not significant after structural correction.

For site NF04, a tepee-like structure at Second Plain, the Scos1 statistic for $N = 8$ increases from 1.0 to 6.3 and the 95% confidence point is 3.3. This suggests that the magnetisation of the Nuccaleena Formation at Second Plain post-dates tepee formation.

The tepee-like structure at site NF07 near the Nuccaleena mine yielded a Scos1 statistic for $N = 10$ that decreased from 4.2 to 2.4, with the 95% confidence point being 3.7. This suggests that the magnetisation of the Nuccaleena Formation near the Nuccaleena mine pre-dates tepee formation. However, the minimum Scos1 was found to be <0.1 at 60% unfolding, suggesting that the magnetisation here was acquired during tepee formation, before the structure was fully developed.

An inconclusive fold test was determined at site NF08 (Angorichina Creek), where Scos1 was 2.5 before unfolding and 2.2 after unfolding, compared to the 95% confidence value of 5.8. The minimum Scos1 was at 100% of unfolding suggesting that the test would be positive but with a low level of confidence. Indeed, examination of directions before and after unfolding showed that some converged while others diverged, reminiscent of the situation we found with magnetisations formed during folding of the Palaeoproterozoic Sokoman Formation, Québec (Williams and Schmidt, 2004a). This will be the basis of an ongoing study to examine in detail the magnetisation of the Nuccaleena tepee-like structures.

All in all, the fold tests from the tepee-like structures may be interpreted as consistent with magnetisation being acquired at or near the time of formation of the structures, with some locali-

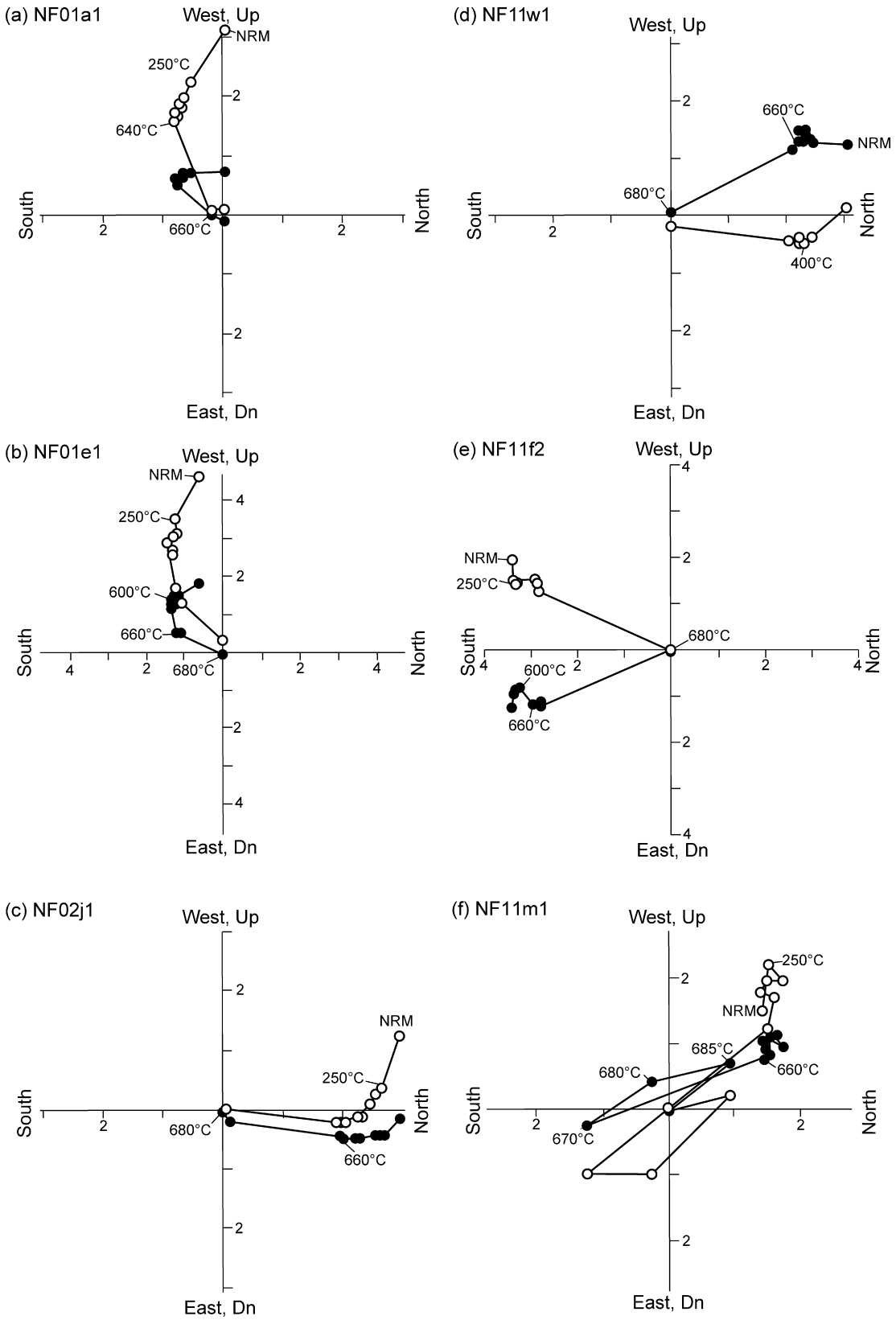

Fig. 4. Orthogonal projections of remanence vectors for specimens of the Nuccaleena Formation after stepwise thermal demagnetisation (°C). Solid circles plot on the horizontal plane and open circles on the vertical plane. Axes are mA m^{-1} ($\times 10^{-6}$ emu cm^{-3}). See text for details.

ties acquiring remanence slightly before, some during and some slightly after the structures formed. We interpret the Nuccaleena remanence as having been acquired during early diagenesis, when the tepee-like structures formed (e.g. Gammon et al., 2005). Remanence probably lagged deposition by approximately the time taken for several metres of deposition—perhaps on the order of 10^5 years. The significance of this result in terms of magnetostratigraphic correlation is considerable, because the time lag

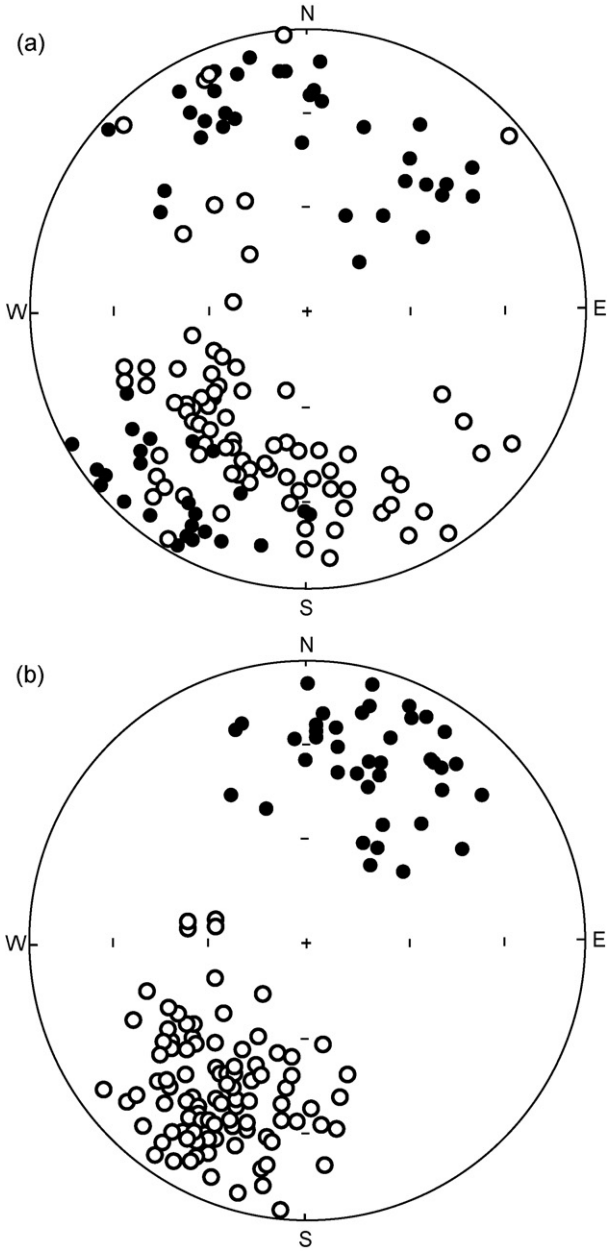

Fig. 5. Stereographic projections of ChRM directions for the Nuccaleena Formation isolated by stepwise thermal demagnetisation. Solid circles plot on the lower hemisphere and open circles on the upper hemisphere: (a) present-day coordinates; (b) after structural correction. The tighter cluster of the latter reflects a positive fold test at 99% confidence and indicates that acquisition of magnetisation occurred before the early Palaeozoic Delamerian Orogeny.

appears to be of similar order to the reversal rate, i.e. the tepee-like structures formed at up to several metres depth whereas the whole Nuccaleena Formation is only ~10 m thick on average. Hence the magnetostratigraphic horizons could be highly bedding-transgressive, making regional correlation invalid. Nevertheless, the number and duration of polarity chrons at various localities may be valid, despite the time lag between deposition and magnetisation. This is because the time lag simply translates into a vertical offset between time-lines represented by the strata and time-lines represented by locking-in of remanence. The offset may vary within site, depending on changing local conditions, as it may also vary between sites, but this need not alter the number of reversals recorded.

4.5. Magnetostratigraphy

Sections at Second Plain (sites NF02 and NF03), Warren Gorge (NF11) and Buckaringa Gorge (NF12) were sampled for magnetostratigraphy. No reliable ChRM was identified from Buckaringa Gorge. Fig. 7 shows declinations for Second Plain and Warren Gorge plotted as a function of stratigraphic height from the base of the lowest dolostone bed of the Nuccaleena Formation. Also shown is the simplified magnetostratigraphy previously determined for the GSSP site by Raub et al. (2007, their Fig. 8). The lowest part of their section is of reverse polarity (SSW declinations), followed by an interval of normal polarity (NNE declinations), changing back to reverse polarity for the topmost part of the section.

The Second Plain sites are ~25 km northeast of the GSSP site, and Warren Gorge (NF11) is ~100 km southwest of the GSSP (Fig. 3). Reliable ChRMs at site NF03 are mostly confined to the top few metres of the section, whereas the magnetostratigraphy for site NF02 is reasonably well defined. The chrons identified at NF02 bear a close resemblance to the magnetostratigraphy of Raub et al. (2007) at the GSSP site, except that the onset of normal polarity at NF02 seems to be ~1 m above base of the formation. The transitions to reverse polarity are very similar at ~4.5 m above the base. A transition back to normal polarity occurs ~10 m above the base at NF02 but it does not appear to have been identified at the GSSP site (Raub et al., 2007). The top of the section at NF03 is reversed, which implies a further transition above the 10 m R–N transition of NF02. This suggests a sequence of R–N–R–N–R at Second Plain, of which the first three chrons R–N–R are in reasonable agreement with the GSSP sequence. Alternatively, the top of NF03 may correlate with the reverse chron from ~5–10 m at NF02. This would imply, however, several metres vertical difference in magnetisation blocking for only a few tens of metres horizontal offset.

The Warren Gorge (site NF11) magnetostratigraphy is reasonably well defined only over the interval 2–8 m above base. This interval is of reverse polarity except between 6 and 7 m where there appear to be rapid oscillations between polarities. These are probably artifacts of the diagenetic origin of the magnetisation (see Section 4.4).

The magnetisation front is unlikely to be sharp and well defined during diagenesis: a general younging of magnetisations occurs upwards, but in detail, older magnetisations could be acquired stratigraphically above younger magnetisations. Thus, while the number of chrons present in sections may be similar, the transitions may not agree exactly, such as the first R–N transitions at the GSSP site and at NF02. Likewise, the R–N transition defined in Warren Gorge may correspond to the 10 m R–N transition at Second Plain (NF02). Being over 100 km distant, magnetisation events at Warren Gorge could be vertically offset by several metres from those at the GSSP site and Second Plain, assuming the base of the Nuccaleena Formation to be broadly synchronous over that distance. Because the magnetisation evidently was acquired during diagenesis near the time that tepee-like structures were developing (see Section 4.4), this is the best resolution possible from the magnetostratigraphy of the Nuccaleena Formation. Raub and Evans (2006), in comparing the magnetostratigraphy of the Puga cap carbonate near Mirassol d'Oeste (Amazon craton) and the Nuccaleena Formation, stated that "... if both paleomagnetic signals are primary then they [the formations] must be diachronous on polarity-zone timescales". We would argue, conversely, that the palaeomagnetic signals are diagenetic, at least for the Nuccaleena Formation, which invalidates attempts at intercontinental lithostratigraphic correlation. Nevertheless, Neoproterozoic cap carbonates appear to have recorded several polarity transitions and would therefore appear to have been deposited over 10^5 to 10^6 years.

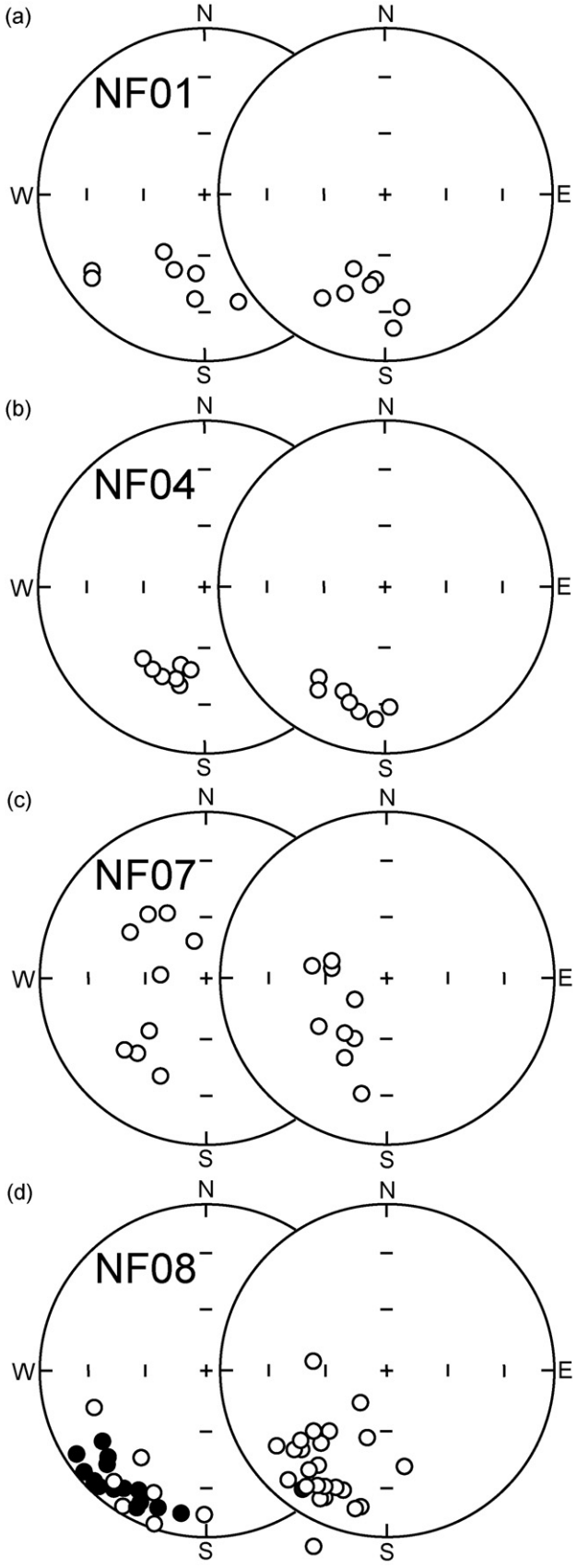

Fig. 6. Stereographic projections of ChRM directions for tepee-like structures in the Nuccaleena Formation, isolated by stepwise thermal demagnetisation. Solid circles plot on the lower hemisphere and open circles on the upper hemisphere. Data for present-day coordinates on the left, and data after structural correction on the right. (a) NF01, GSSP site in Enorama Creek, positive fold test at 95% confidence; (b) NF04, Second Plain, negative fold test; (c) NF07, near Nuccaleena Mine, positive fold test at 95% confidence for 60% unfolding; (d) NF08, Angorichina Creek, inconclusive fold test. The mixture of pre-, syn- and post-folding is interpreted to indicate that acquisition of magnetisation occurred for a prolonged interval after deposition, during diagenesis.

Table 2
Summary of anisotropy of magnetic susceptibility.

Rock unit	*N*	Dec (°)	Inc (°)	k ($\times 10^{-6}$ SI)	*A*	*L*	*F*	*t*
Nuccaleena dolostones								
k_1	16	331.6	18.3	50.3	1.032	1.020	1.012	−0.265
k_2		207.6	59.4	49.3				
k_3		70.0	23.6	48.7				
Elatina tidal rhythmites								
k_1	12	171.2	18.3	117.0	1.021	1.017	1.004	−0.609
k_2		261.9	2.3	115.1				
k_3		358.7	71.5	114.6				
Elatina arenites								
k_1	44	45.1	29.4	116.5	1.042	1.009	1.033	0.575
k_2		304.8	17.6	115.4				
k_3		188.2	54.8	111.7				

A, anisotropy (k_1/k_3); *L*, lineation (k_1/k_2); *F*, foliation (k_2/k_3); *t*, shape factor $(2\eta_2 - \eta_1 - \eta_3)/(\eta_1 - \eta_3)$ where $\eta_i = \ln(\tau_i)$ and τ_i is the *i*th eigenvalue of the normalized susceptibility tensor (Jelinek, 1981).

5. The question of inclination shallowing

5.1. Anisotropy of magnetic susceptibility and remanence

To estimate any compaction-related inclination shallowing, one measure that is relevant is the anisotropy of magnetic susceptibility (AMS). AMS data for specimens from the Nuccaleena and the Elatina formations are summarised in Table 2. Specimens from the Nuccaleena Formation comprised silty, microcrystalline dolostone, and those from the Elatina Formation medium- and coarse-grained sandstone and tidal rhythmites of siltstone and fine-grained sandstone (Williams, 1991, 2000; Williams et al., 2008, in press). The Nuccaleena dolostones and the Elatina tidal rhythmites both display a dominant lineation directed along a shallow north–south axis, whereas the dominant anisotropy of the Elatina coarser-grained, arenaceous specimens is a foliation with the minimum, k_3, steeply inclined and possibly reflecting a weak compaction fabric. The AMS of all the specimens is low, less than ~4%; such values imply minimal inclination shallowing (Enkin et al., 2003). Interestingly, the north–south lineation is similar to that reported by Li and Powell (1993) for nearby Cambrian rocks, which they interpreted as the intersection between a bedding-parallel foliation and a north–south trending sub-vertical tectonic foliation.

Possible inclination shallowing in sedimentary rocks has been recognised since they were first studied palaeomagnetically by King (1955), who used the following relationship to quantitatively describe the effect:

$$\tan I_0 = f \tan I_f \quad (2)$$

where f is the "flattening factor", I_0 is the palaeomagnetic inclination and I_f is the inclination of the palaeomagnetic field. Jackson et al. (1991) showed that f is related to the anisotropy of depositional remanent magnetisation (DRM) according to:

$$f = \frac{k_{D3}}{k_{D1}} \quad (3)$$

where k_{D1} is the magnitude of the maximum DRM anisotropy axis in the bedding plane, and k_{D3} is the minimum, usually perpendicular to bedding. Because it is extremely difficult, if not impossible,

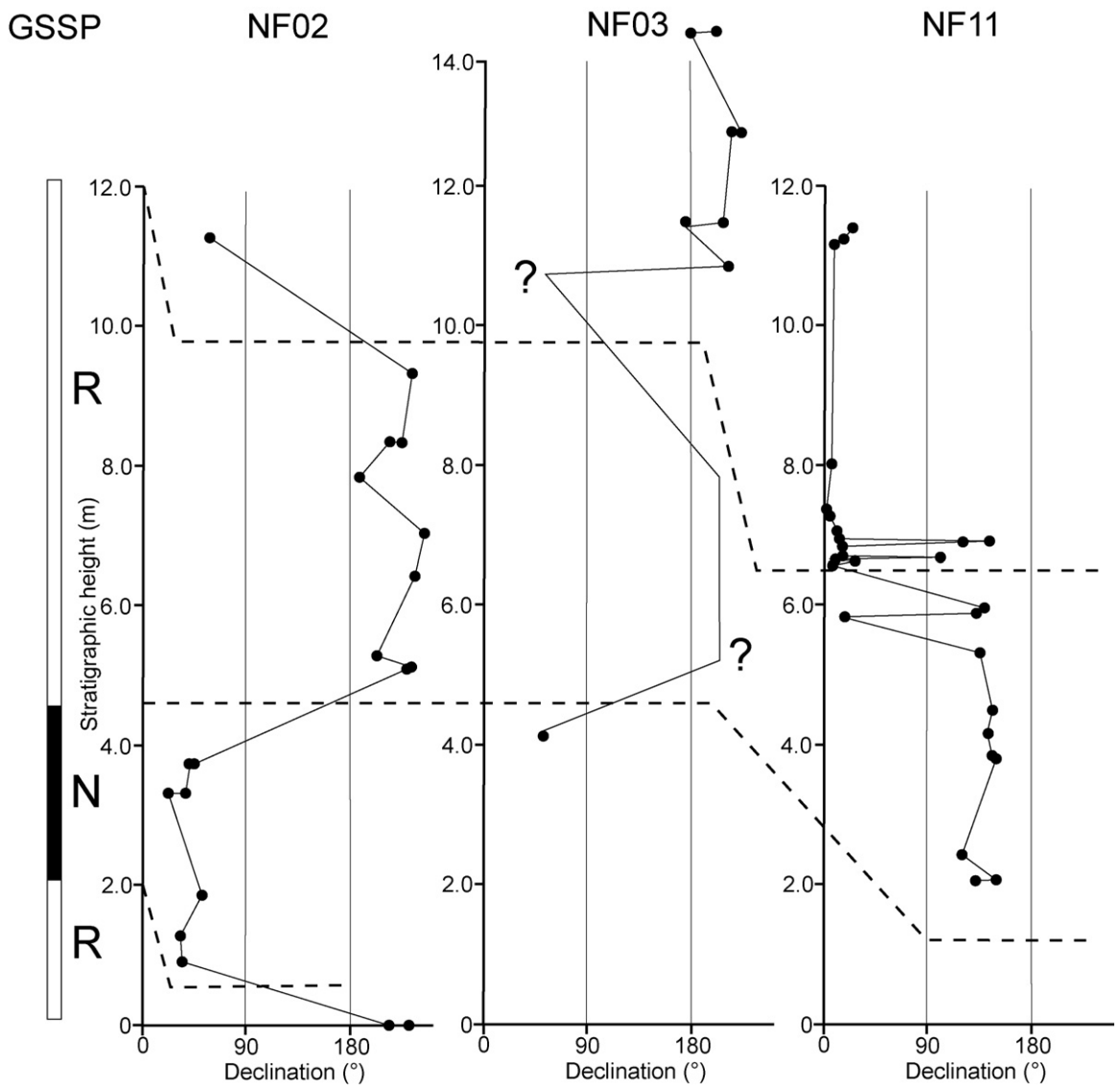

Fig. 7. Magnetostratigraphy of the Nuccaleena Formation for sections at Second Plain (NF02 and NF03) and Warren Gorge (NF11) compared to that reported for the GSSP site in Enorama Creek (Raub et al., 2007). The base of the Nuccaleena Formation is taken to be synchronous within the study area. N, normal polarity; R, reverse polarity.

to determine DRM anisotropy experimentally, a proxy is used. For magnetite-bearing rocks, either thermoremanent magnetisation (TRM) or anhysteretic remanent magnetisation (ARM) is used. ARM is often preferred, to avoid thermochemical alteration of the sample which violates the experimental assumptions that each acquisition is equal except for the susceptibility along each axis.

Finding a k_D proxy for hematite-bearing rocks is problematical. The principal issue is the history of previous magnetisations, which can be easily erased in magnetite-bearing rocks by AF demagnetisation. The prohibitively high coercivity of hematite rules out AF demagnetisation. Consequently, only a fraction of the coercivity spectrum is accessible, leaving a significant memory from previous exposures to high magnetic fields. By using a 14 T magnet, Kodama and Dekkers (2004) demonstrated that it is possible to derive the full anisotropy tensor for hematite-bearing samples by imparting saturation isothermal remanent magnetisation (IRM), which activates almost the whole coercivity spectrum.

To determine the flattening factor, *f*, the full tensor is not required because of symmetry (Eq. (3)), but it is necessary to know the bedding plane to determine k_{D1} and k_{D3} directly. We have imparted saturation IRMs using a 12 T field from a superconducting magnet along the *x*, *y* and *z* axes of specimens, where *x* and *y* are in the bedding plane and *z* is perpendicular to bedding. There will be a small bias towards low values for *f* because this method does not guarantee that k_{D1}, the maximum susceptibility, in the bedding plane will be determined. However, the bedding-plane anisotropy of a few specimens was measured and shown to be very low ($\ll$1%), so it is unlikely that the bias is significant.

The results of the 12 T saturation IRMs are listed in Tables 3–5, for the Nuccaleena dolostones, Elatina tidal rhythmites and Elatina

Table 3
Nuccaleena dolostones—anisotropy of 12 T J_s.

Specimen	k_{D1} (mA m^{-1})	k_{D3} (mA m^{-1})	k_{D3}/k_{D1}
01a2	4011.1	4026.6	1.00
01a6	5692.1	5536.1	0.97
01c1	2719.2	2670.1	0.98
01d2	4231.1	4115.1	0.97
Mean	4163.3	4087.0	0.98
Std dev.	1218.0	1170.7	0.015
SD%	29.3	28.6	1.5

k_{D1}, magnitude of the maximum DRM anisotropy axis in the bedding plane; k_{D3}, minimum DRM anisotropy axis, usually perpendicular to bedding.

Table 4
Elatina tidal rhythmites—anisotropy of 12 T J_s.

Specimen	k_{D1} (mA m^{-1})	k_{D3} (mA m^{-1})	k_{D3}/k_{D1}
A7B1a	5119.1	5001.3	0.98
PR2a	5393.3	5222.0	0.97
A8b1a	5146.2	4998.7	0.97
PR11b	5130.5	4976.5	0.97
B5B1a	5447.4	5337.4	0.98
B5B1b	5470.2	5345.4	0.98
Mean	5284.5	5146.9	0.97
Std dev.	169.1	175.2	0.005
SD%	3.2	3.4	0.5

See footnote to Table 3 for explanation of k_{D1} and k_{D3}.

arenites, respectively. The mean flattening factor and number of specimens for the units investigated are as follows.

Nuccaleena dolostones: $N = 4$; $f = 0.98 \pm 0.02$.
Elatina tidal rhythmites: $N = 6$; $f = 0.97 \pm 0.01$.
Elatina arenites: $N = 9$; $f = 0.92 \pm 0.02$.

Using Eq. (2) to correct for inclination flattening or shallowing makes little difference to the palaeomagnetically determined inclinations, partly because the palaeomagnetically determined inclinations are already quite low. The inclination of −34.9° for the Nuccaleena Formation is corrected to −35.4° (palaeolatitude of 19.6°) and the mean Elatina Formation inclination of −12.9° is corrected to −14.0° (palaeolatitude of 7.1°). Recalling that k_{D1} may not be precisely the maximum susceptibility in the bedding plane, it is instructive to examine the worst cases to gain an appreciation of how sensitive the solutions are to extreme values. For the Nuccaleena dolostones and the Elatina tidal rhythmites, the standard deviations are negligible. The worst case for the Elatina arenites may be expected to be close to the maximum k_{D1} since $N = 9$, and assuming a uniform distribution of sampled axes in the bedding plane it is unlikely that from this number of random measurements that k_{D1} has been completely elusive. The extreme value for the Elatina arenites is $f = 0.90$ (Table 5). According to Eq. (3) this value changes inclination from −12° to −13.3°. Clearly, the above corrections for inclination shallowing due to compaction, or other effects, do not materially affect the palaeolatitude of the Elatina Formation and the case for low-palaeolatitude glaciation.

5.2. Elongation–Inclination method

A method recently developed to investigate evidence for inclination shallowing compares palaeomagnetic directions with geomagnetic models for 0–5 Ma (Tauxe and Kent, 2004). Virtual geomagnetic poles (VGPs) are circularly distributed; because of the dipole inclination–latitude relationship, palaeomagnetic directions are transformed into vertically elongate distributions which depend on latitude, tending to result in circular distributions at high latitudes. Elongation is defined as the ratio of the intermediate to the smallest eigenvalue of the distribution of palaeomagnetic vectors expressed after combining all directions in the same polarity.

At equatorial latitudes, elongations of 2.9 are expected if the geomagnetic field is similar to the average behaviour observed for 0–5 Ma. The Tauxe–Kent method makes use of Eq. (2), which relates inclination shallowing (f) to the geomagnetic field inclination, to increment f and observe the change in elongation of each distribution. At the point where the elongation equals the geomagnetic field model (here TK03 is used; Tauxe and Kent, 2004), the inclination is the same as the geomagnetic field at the time of remanence acquisition, and the value of f is the amount of flattening that has occurred.

We applied the Tauxe–Kent method to the Nuccaleena and the Elatina formations and the results are plotted in Fig. 8. On the left side are structurally and bedding-corrected distributions plotted on equal-area projections rotated so the mean direction is at the centre, aligned with the positive x direction and the negative z direction upward, so the vertical orientation of the elongations with respect to bedding is retained. For both the Nuccaleena and Elatina formations the upper projection corresponds to remanence direction with $f = 1$, that is, as measured. The lower projections correspond to the distributions at the point where their elongations conform to the 0–5 Ma model TK03.

For the Nuccaleena Formation, the elongation of ∼1.7 is in the bedding plane and the inclination is ∼36°, as measured. After varying f until the elongation conforms to TK03, a vertically oriented elongation of ∼1.86 and an inclination of ∼43° is calculated. For combined data for the Elatina Formation the elongation also is ∼1.7, somewhat skewed out of the bedding plane. After incrementing f until the elongation conforms to TK03, elongation is ∼2.47, more vertically oriented, and the inclination is ∼19°.

The Tauxe–Kent method suggests that the geomagnetic-field inclination at the time of deposition of the Nuccaleena Formation was 43°, corresponding to a palaeolatitude of 25°, i.e. an increase of ∼6° over the directly observed value. For the Elatina Formation, the apparent geomagnetic field inclination at the time of deposition according to the Tauxe–Kent method was 19°, corresponding to a palaeolatitude of 9.8°, i.e. an increase of a slightly more than 3°. The skewed distribution of the observed distribution for the Elatina Formation detracts somewhat from its suitability for the Tauxe–Kent method. Tauxe et al. (2008) emphasised that the method assumes only two sources of scatter; variations in the geomagnetic field and sedimentary flattening. This dataset may be contaminated with small secondary magnetisations that have not been entirely eliminated by thermal cleaning and so may not be suitable for the Elongation–Inclination method.

The implied small increases in inclination for the Elatina Formation do not materially change the argument that the Elatina glaciation occurred in low palaeolatitudes. The palaeolatitude of the Nuccaleena Formation, however, appears to be significantly higher than that of the Elatina Formation, as indicated also in Section 5.1. The possible implications of this are discussed below.

Table 5
Elatina arenites—anisotropy of 12 T J_s.

Specimen	k_{D1} (mA m^{-1})	k_{D3} (mA m^{-1})	k_{D3}/k_{D1}
20c2	10,630.7	10,100.0	0.95
22a3	12,875.4	11,697.4	0.91
23a1	23,512.3	22,722.5	0.97
24a2	8,027.0	7,277.6	0.91
27d1a	9,354.7	8,588.9	0.92
27d1b	6,646.1	6,242.0	0.94
27d2	7,777.0	7,154.7	0.92
27d4	5,980.0	5,390.6	0.90
27f2	7,689.6	6,967.4	0.91
Mean	10,277.0	9,571.2	0.92
Std dev.	5,391.6	5,305.2	0.023
SD%	52.5	55.4	2.4

See footnote to Table 3 for explanation of k_{D1} and k_{D3}.

5.3. Cross-bedding dip angle and compaction

Cross-bedding dip angle can provide a measure of sandstone vertical compaction (Rittenhouse, 1972; Borradaile, 1973; Corey et al., 2005). Natural gravels and sands have angles of rest or repose (residual angles after shearing) generally in the range of 30–35°, which is independent of the intergranular fluid (Allen, 1982, pp. 61–62). Bagnold (1965, p. 201) gave the maximum angle of repose

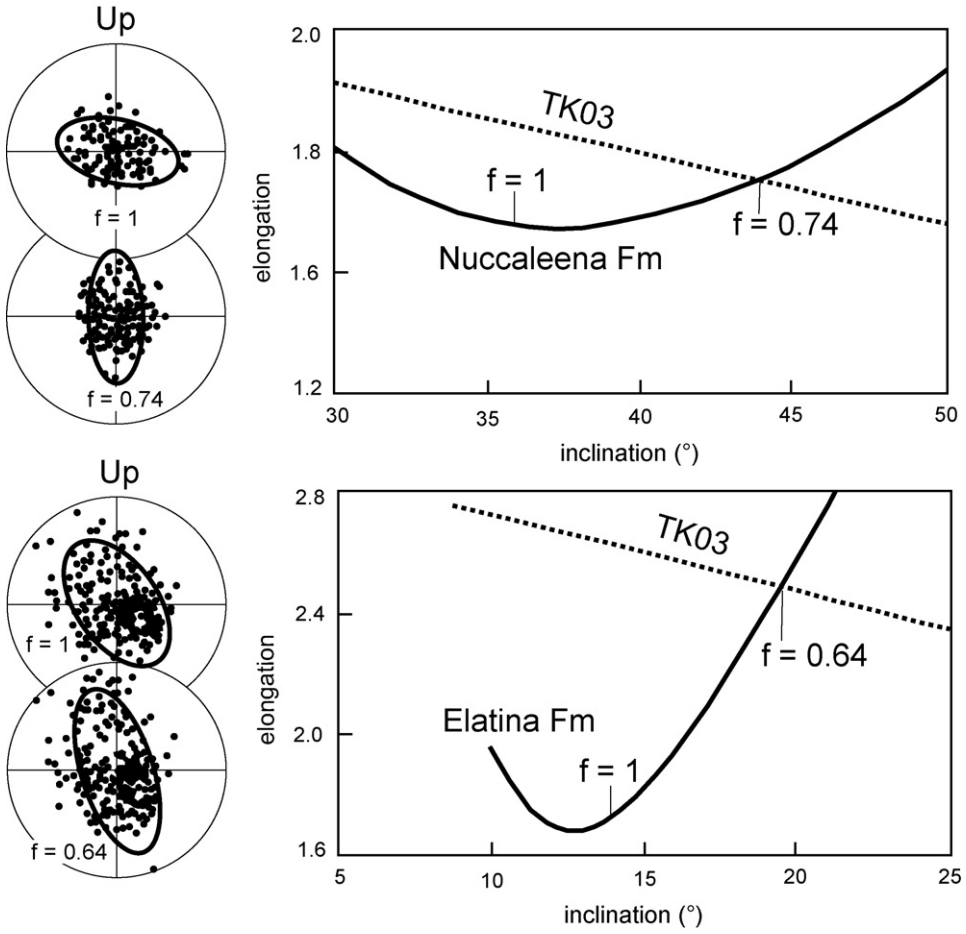

Fig. 8. Elongation–Inclination plots for the Nuccaleena and Elatina formations, after the method of Tauxe and Kent (2004). Because virtual geomagnetic poles (VGPs) are circularly distributed, the dipole inclination–latitude relationship transforms palaeomagnetic directions into vertically elongate distributions whose ellipticity depends on latitude, tending to circular distributions at high latitudes. For distributions that are also affected by inclination shallowing due to compaction, it is possible to make incremental inclination corrections by applying the flattening formula of King (1955) until the ellipticity expected from a model (here we use the TK03 model) is obtained. The method predicts that once the ellipticity is correct then the directions have also been corrected for any inclination shallowing. Plots on the left are stereographic projections onto a vertical section to show the distributions in situ and for the optimal flattening factor to conform to the TK03 ellipticity.

of sand as 34°. Hence the dip angle of sandstone cross-strata that are unaffected by soft-sediment or tectonic deformation, measured relative to associated flat-bedding and compared to a maximum possible angle of 35°, can provide an upper limit on post-depositional vertical compaction. The maximum angle of repose is for loosely packed surficial sediment prior to burial, and hence calculations using cross-bedding dip angles overestimate the upper limits on vertical compaction and inclination shallowing since early diagenesis when an early CRM may be acquired.

Dip angles of up to 24–26° were observed for undeformed cross-strata in medium- to coarse-grained sandstones from the Elatina Formation and the underlying Wilmington Formation in Pichi Richi Pass and the Elatina Formation in Brachina and Mount Chambers creeks, indicating an upper limit on vertical compaction of 30–36%. Employing that upper limit, the determined Elatina palaeomagnetic inclination of 12.9° for combined data is increased to 18.4–20.2°, which gives an upper limit of 9.4–10.4° for the palaeolatitude of the Elatina Formation. This finding is consistent with the rock magnetic data given above.

For the determined Elatina inclination and palaeolatitude, which mostly are for arenaceous sediments, to equate with those for the Nuccaleena Formation would require unreasonably high vertical compaction for the Elatina Formation: 67% vertical compaction for the Nuccaleena palaeomagnetic data reported herein, and 54% vertical compaction for the Nuccaleena data of Raub and Evans (2008). These figures far exceed the estimated upper limit on vertical compaction based on cross-bedding dip angle. We conclude that the difference in inclination and palaeolatitude between the Elatina and Nuccaleena formations cannot be ascribed to compaction-related inclination shallowing for the Elatina Formation.

5.4. Compaction of mudstones

A direct estimate of differential inclination shallowing for mudstones can be made by examining the directions carried by the transition beds of carbonate and interbedded mudstone at the top of the Nuccaleena Formation and base of the Brachina Formation, such as at site NF11. Separating the 43 samples from site NF11 by lithology, the following mean directions were obtained: carbonate ($N = 30$), $D = 194.1°$, $I = -33.6°$ ($\alpha_{95} = 7.7°$); mudstone ($N = 10$), $D = 195.8°$, $I = -21.1°$ ($\alpha_{95} = 7.8°$); and mixed carbonate/mudstone ($N = 3$), $D = 201.9°$, $I = -13.2°$ ($\alpha_{95} = 24.8°$). The steeper mean inclination found in the carbonate samples compared to that for the mudstone samples suggests that the mudstone may have experienced some inclination shallowing. However, the cones of confidence of the two mean directions overlap markedly, so a statistical test is required. The mean directions of the carbonate and the mudstone samples can be compared using the test of McFadden and Lowes (1981, Eq. (25)). The relevant statistic has a value of 2.59, which for $N = 40$ is less than $F_{2,76} = 3.12$, indicating that the

directions for the carbonate and mudstone are statistically indistinguishable with 95% confidence. Whereas inclination shallowing may have affected the mudstone more than the carbonates, the effect is not significant for these samples. As noted above, however, our samples from the Elatina Formation did not include mud rocks.

6. Discussion

6.1. Reversal frequency and time constraints

Taken at face value, our findings herein and those for other cap carbonates (see Section 2) imply that recovery from glacial conditions occurred over long time-scales, possibly >10^5 to 10^6 years, and that cap carbonates accumulated slowly (<0.1–0.01 mm year^{-1}, on average, for an actualistic reversal frequency).

Stratigraphic control for the position of polarity transitions is documented for the Puga and Hadash cap carbonates (Trindade et al., 2003; Kilner et al., 2005) and the Nuccaleena Formation (Raub and Evans, 2006). Although no convincing correlations of these transitions have been demonstrated, probably because of the lag between deposition and magnetisation discussed above, the transitions are relevant to the duration of cap carbonate deposition. Hoffman et al. (2007) estimated that a full change of polarity (transition) in the Nuccaleena Formation spans 10 cm and suggested that this thickness represents ~5×10^3 years; they then estimated a duration of 2.5×10^5 years for a 5 m thick cap carbonate. Hoffman et al. (2007) regarded this interval as too long to be accommodated in the rapid deglaciation scenario required by the snowball Earth hypothesis, suggesting instead that the frequency and speed of polarity transitions for the late Neoproterozoic were 1–2 orders of magnitude greater than those for the past 300 million years. If so, 10 cm Nuccaleena polarity transition zones would represent hundreds of years or less, rather than the thousands of years observed for Phanerozoic transitions, and the whole 5 m thick cap carbonate would represent perhaps only a few tens of thousands of years. Examining the geomagnetic polarity chrons from marine magnetic anomalies presented by Gee and Kent (2007), in the past 160 million years there have been only 12 chrons out of about 300 that were shorter than 3.0×10^4 years. The chances of several such short chrons occurring consecutively are exceedingly small. This is especially so considering the accumulating evidence that secular variation and the rate of geomagnetic reversals were reduced in the Precambrian (Roberts and Piper, 1989; Halls, 1991; Gallet et al., 2000; Elston et al., 2002; Strik et al., 2003; Dunlop and Yu, 2004; Biggin et al., 2008), in addition to the independent modelling by Coe and Glatzmaier (2006) which showed that a smaller inner core in the Precambrian would lead to fewer geomagnetic reversals. Therefore the longer estimate of ~2.5×10^5 years for Nuccaleena deposition is more consistent with the number of chrons indicated by the palaeomagnetic data.

Table 6
Palaeolatitudes for Cryogenian and Ediacaran sedimentary rocks from the Adelaide Geosyncline and Officer Basin, southern Australia.

Formation (depth, m)	Age (Ma)	Lithology	Palaeolatitude (°) Single polarity	Dual polarities	Locality	Reference
Wonoka Fm	~570	Siltstone, calcareous siltstone, limestone	12.4 + 3.8/−3.5		Adelaide Geosyncline	(5)
Bunyeroo Fm	~580	Siltstone, mudstone	15.7 + 7.1/−6.1		Adelaide Geosyncline	(6)
Brachina Fm	~600	Siltstone, mudstone, minor fine-grained sandstone	11.8 ± 2.5		Adelaide Geosyncline	(5)
Nuccaleena Fm	<635	Dolostone	19.2 + 2.3/−2.2		Adelaide Geosyncline	(5)
Nuccaleena Fm	<635	Dolostone	14 ± 2		Adelaide Geosyncline	(7)
Elatina Fm	~635	Sandstone, siltstone	6.5 ± 2.2		Adelaide Geosyncline	(4)
Wahlgu	~635	Diamictite	7.3 ± 16.5		Lancer 1, Officer Basin	(2)
Lupton Fm	~635	Sandstone, mudstone, diamictite	0.6 ± 4.7	10.9 ± 2.5	Empress 1A, Officer Basin	(1)
Yaltipena Fm	>635	Sandstone, mudstone	8.4 + 6.2/−5.7		Adelaide Geosyncline	(3)
Steptoe Fm	~720	Sandstone, mudstone, dolostone	6.5 ± 5.8	11.6 ± 3.4	Empress 1A, Officer Basin	(1)
Kanpa Fm	760–720	Sandstone, mudstone	9.1 + 8.3/−7.4		Lancer 1, Officer Basin	(2)
Kanpa Fm (621–667)	760–720	Dolostone, mudstone, sandstone	7.3 ± 8.0	11.1 ± 5.7	Empress 1A, Officer Basin	(1)
Kanpa Fm (670–731)	760–720	Dolostone, mudstone, sandstone	1.5 ± 8.2	8.6 ± 4.4	Empress 1A, Officer Basin	(1)
Kanpa Fm (735–785)	760–720	Dolostone, mudstone, sandstone	4.9 ± 9.2	8.9 ± 5.8	Empress 1A, Officer Basin	(1)
Kanpa Fm (789–857)	760–720	Dolostone, mudstone, sandstone	3.5 ± 17.5	15.0 ± 8.0	Empress 1A, Officer Basin	(1)
Hussar Fm	800–760	Sandstone, mudstone	2.3 ± 9.9		Lancer 1, Officer Basin	(2)
Hussar Fm (860–1041)	800–760	Sandstone, dolostone, mudstone	0.1 ± 7.8	14.8 ± 4.1	Empress 1A, Officer Basin	(1)
Hussar Fm (1046–1101)	800–760	Sandstone, dolostone, mudstone	0.8 ± 12.8	7.5 ± 7.1	Empress 1A, Officer Basin	(1)
Hussar Fm (1106–1151)	800–760	Sandstone, dolostone, mudstone	7.4 ± 21.9	12.5 ± 12.3	Empress 1A, Officer Basin	(1)
Hussar Fm (1153–1246)	800–760	Sandstone, dolostone, mudstone	9.6 ± 9.2	16.5 ± 5.3	Empress 1A, Officer Basin	(1)
Browne Fm	830–800	Mudstone, siltstone, sandstone	18.5 + 5.5/−4.9		Lancer 1, Officer Basin	(2)
Browne Fm	830–800	Siliciclastics, evaporites, stromatolitic dolostone	10.6 ± 6.1	13.4 ± 4.1	Empress 1A, Officer Basin	(1)

References: (1) Pisarevsky et al. (2001); (2) Pisarevsky et al. (2007); (3) Sohl et al. (1999); (4) herein and Williams et al. (2008, in press); (5) Herein; (6) Schmidt and Williams (1996); (7) Raub and Evans (2008). Ages for formations from the Officer Basin based on Grey et al. (2005) and Pisarevsky et al. (2007). See Table 7 for data for the Brachina and Wonoka formations.

6.2. Elatina–Nuccaleena inclination difference

Palaeomagnetic studies of the Elatina Formation (Embleton and Williams, 1986; Schmidt et al., 1991; Schmidt and Williams, 1995; Sohl et al., 1999) and the Nuccaleena Formation have identified several polarity chrons in each formation, indicating that results represent sufficient time to provide mean directions free of bias from secular variation. Unless the Neoproterozoic field was characterised by large non-dipole components that changed over time-scales similar to the difference in age of these units, the source of the inclination difference between the Elatina and the Nuccaleena formations remains to be explained.

The mean palaeomagnetic inclination for combined data for the Elatina Formation (Schmidt and Williams, 1995; Sohl et al., 1999) is $-12.9 \pm 4.2^\circ$ (herein and Williams et al., 2008, in press), yielding a palaeolatitude range of 5–9°, compared to a mean inclination of $-34.9 \pm 3.4^\circ$ and a palaeolatitude range of 17–22° for the Nuccaleena Formation (Table 1). The minimum palaeolatitude difference at the 95% confidence limit is 8°. For a landmass drifting south at 10 cm year^{-1} and assuming an axial geocentric dipole field, this minimum difference would represent ~9 million years. Taking a minimum peak rate of 16–18 cm year^{-1} for plate motion (Meert et al., 1993) gives a time interval of less than 5–6 million years. If a palaeolatitude of $14 \pm 2^\circ$ (inclination of $26.5 \pm 3^\circ$) is employed for the Nuccaleena Formation, as given by Raub and Evans (2008), the time interval is reduced to ~3 million years for a drift rate of 10 cm year^{-1} and much less for faster plate motions. The disconformity to low-angle unconformity below the Nuccaleena Formation (Fig. 2e) is a basin-wide sequence boundary (Preiss, 2000; Williams et al., 2008) that cuts deeply into the ~1500 m thick, late Cryogenian glaciogenic Yerelina Subgroup in parts of the northern Adelaide Geosyncline (Coats and Blissett, 1971; Coats et al., 1969, 1973; Ambrose, 1973) and may represent a significant time gap. In the southern Adelaide Geosyncline, the pale red and grey Seacliff Sandstone sharply overlies the Elatina Formation, and the principal dolostone unit of the Nuccaleena Formation occurs 70 m stratigraphically above the Elatina (Forbes and Preiss, 1987). Elsewhere in the southern Adelaide Geosyncline the Seacliff Sandstone attains a thickness of 340 m and intertongues with the Nuccaleena Formation and overlying Brachina Formation (Forbes and Preiss, 1987; Preiss, 1993). Hence the late Cryogenian–Ediacaran sequence boundary in South Australia marks a major hiatus with a significant time break between Elatina and Nuccaleena deposition. Significantly, Zhang et al. (2008) found an extensive (>500 km) claystone between the late Cryogenian glaciogenic Nantuo Formation and its overlying Doushantuo cap carbonate in south China, which they interpreted as indicating "a time lag between the end of the Nantuo deglaciation and cap carbonate precipitation". Hence the question perhaps is not one of inclination-shallowing but rather the time represented by the sequence boundary between the Elatina and Nuccaleena formations and the rate of coincident plate motion or polar wander.

6.3. Palaeolatitudes of Neoproterozoic strata in southern Australia

Palaeolatitudes determined for Cryogenian and Ediacaran sedimentary rocks from the Adelaide Geosyncline and the central Officer Basin, both in southern Australia, are listed in Table 6 and plotted in Fig. 9. The general trends seem to be movement from ~10–20° palaeolatitude in the early Cryogenian (850–750 Ma, non-glacial times), to ~10° for the late Cryogenian (750 to ~635 Ma, glacial times), and a return to higher palaeolatitudes (~10–20°) for the Ediacaran. The trends are not controlled by lithology, with no systematic relationship evident among palaeolatitudes for clastics, mixed clastics and carbonates, and carbonates. Moreover, the palaeomagnetic direction for the Walsh Tillite cap carbonate ($D = 149^\circ$, $I = -63^\circ$, $\alpha_{95} = 10^\circ$) found by Li (2000) is very close to that determined by McWilliams (1977) for siltstone and fine-grained sandstone of the overlying Neoproterozoic Estaughs Formation ($D = 147^\circ$, $I = -62^\circ$, $\alpha_{95} = 14^\circ$), further arguing against preferential inclination-shallowing in clastic beds as compared to carbonates.

6.4. Neoproterozoic–early Palaeozoic pole paths

Palaeomagnetic studies of Cryogenian to post-Delamerian Orogeny rock units from the Adelaide Geosyncline have been filtered using the quality factor Q of Van der Voo (1990). The pole positions that rate at least five (out of a possible seven) criteria are

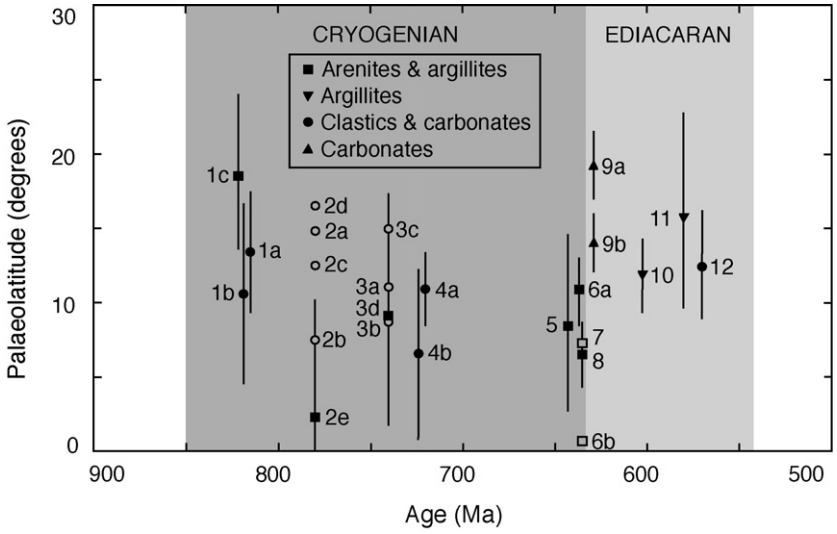

Fig. 9. Palaeolatitudes for Cryogenian and Ediacaran sedimentary rocks from the Adelaide Geosyncline and Officer Basin, southern Australia (solid symbols with error bars, open symbols without error bars): (1a) Browne Fm dual polarities, (1b) single polarity (Pisarevsky et al., 2001); (1c) Browne Fm (Pisarevsky et al., 2007); (2a) Hussar Fm dual polarities, 860–1041 m, (2b) 1046–1101 m, (2c) 1106–1151 m, (2d) 1153–1246 m (Pisarevsky et al., 2001); (2e) Hussar Fm (Pisarevsky et al., 2007); (3a) Kanpa Fm dual polarities, 621–667 m, (3b) 670–785 m, (3c) 789–857 m (Pisarevsky et al., 2001); (3d) Kanpa Fm (Pisarevsky et al., 2007); (4a) Steptoe Fm dual polarities, (4b) single polarity (Pisarevsky et al., 2001); (5) Yaltipena Fm (Sohl et al., 1999); (6a) Lupton Fm dual polarities, (6b) single polarity (Pisarevsky et al., 2001); (7) Wahlgu Fm (Pisarevsky et al., 2007); (8) Elatina Fm (herein and Williams et al., 2008, in press); (9a) Nuccaleena Fm (herein), (9b) Nuccaleena Fm (Raub and Evans, 2008); (10) Brachina Fm (herein); (11) Bunyeroo Fm (Schmidt and Williams, 1996); (12) Wonoka Fm (herein). See Table 6 for details.

Table 7
Summary of reliable late Cryogenian to post-Delamerian Orogeny poles for late Neoproterozoic and early Palaeozoic rocks, South Australia (quality factor Q at least 5/7).

Formation	Dec (°)	Inc (°)	α_{95} (°)	λ_p (°)	φ_p (°)	dp (°)	dm (°)	1	2	3	4	5	6	7	Q	Ref.
Black Hill Norite	231.1	19.7	3.8	−37.5	34.4	3.0	6.0	√	√	√	√	√	×	√	6	a
Lake Frome (basal)	232.3	−0.5	10.1	−31.4	36.9	5.1	10.1	√	√	√	√	√	√	√	6	b
Kangaroo Is red beds	224.5	−4.4	12.3	−33.8	15.1	6.2	12.3	√	√	√	√	√	√	√	6	b
Billy Ck Fm	224.1	−1.2	14.4	−37.4	20.1	7.2	14.4	√	√	√	×	√	√	√	6	b
Hawker Group	233.4	−27.8	11.4	−21.3	14.9	6.8	12.5	√	√	√	×	√	√	√	6	b
Wonoka Fm	255.9	−23.7	6.4	−5.2	30.5	3.6	6.8	×	√	√	√	√	√	√	6	herein
Bunyeroo Fm	236.6	−29.3	10.7	−18.1	16.3	6.5	11.8	×	√	√	√	√	√	×	5	c
Brachina Fm	178.2	−22.6	4.4	−46.0	315.4	2.4	4.6	×	√	√	√	√	√	√	6	herein
Nuccaleena Fm	208.3	−34.9	3.4	−32.3	350.8	2.2	3.9	×	√	√	√	√	√	√	6	herein
Elatina Fm	208.3	−12.9	4.2	−43.7	359.3	2.1	4.2	×	√	√	√	√	√	√	6	herein
Yaltipena Fm	204.0	−16.4	11.0	−44.2	352.7	5.9	11.4	×	√	√	√	√	√	√	6	d

1–7 and Q, Reliability criteria of Van der Voo (1990). a, Schmidt et al. (1993); b, Klootwijk (1980); c, Schmidt and Williams (1996); d, Sohl et al. (1999). Wonoka Fm, $N = 70$; Brachina Fm, $N = 91$. See Table 1 for explanations of other symbols.
Note: Trindade and Macouin (2007) assigned Q = 4 and 6 to the Elatina Formation studies by Schmidt and Williams (1995) and Sohl et al. (1999), respectively. Curiously, Trindade and Macouin (2007) penalised the former study on the grounds that the pole resembles younger palaeopoles (criterion 7). We would argue, however, that because both Elatina palaeopoles are similar they should receive the same classification for criterion 7. Moreover, as Van der Voo (1990) added the caveat that poles should only be ranked zero if they resemble *much* younger palaeopoles, both Elatina studies should be credited for criterion 7. We further argue that only Schmidt and Williams (1995) should be credited with a field test (criterion 4) based on the assertions of Meert and Van der Voo (1994) (also Williams et al., 1995) that a positive fold test (criterion 4) is a significant constraint only if the folding closely follows deposition. The Schmidt and Williams (1995) fold is a soft-sediment structure associated with deposition, whereas Sohl et al. (1999) used Cambrian tectonic folds post-dating deposition by > 100 million years. Thus individually both studies should score Q = 5, but the combined data (see text) scores Q = 6, failing to be credited only for criterion 1, a well-determined age.

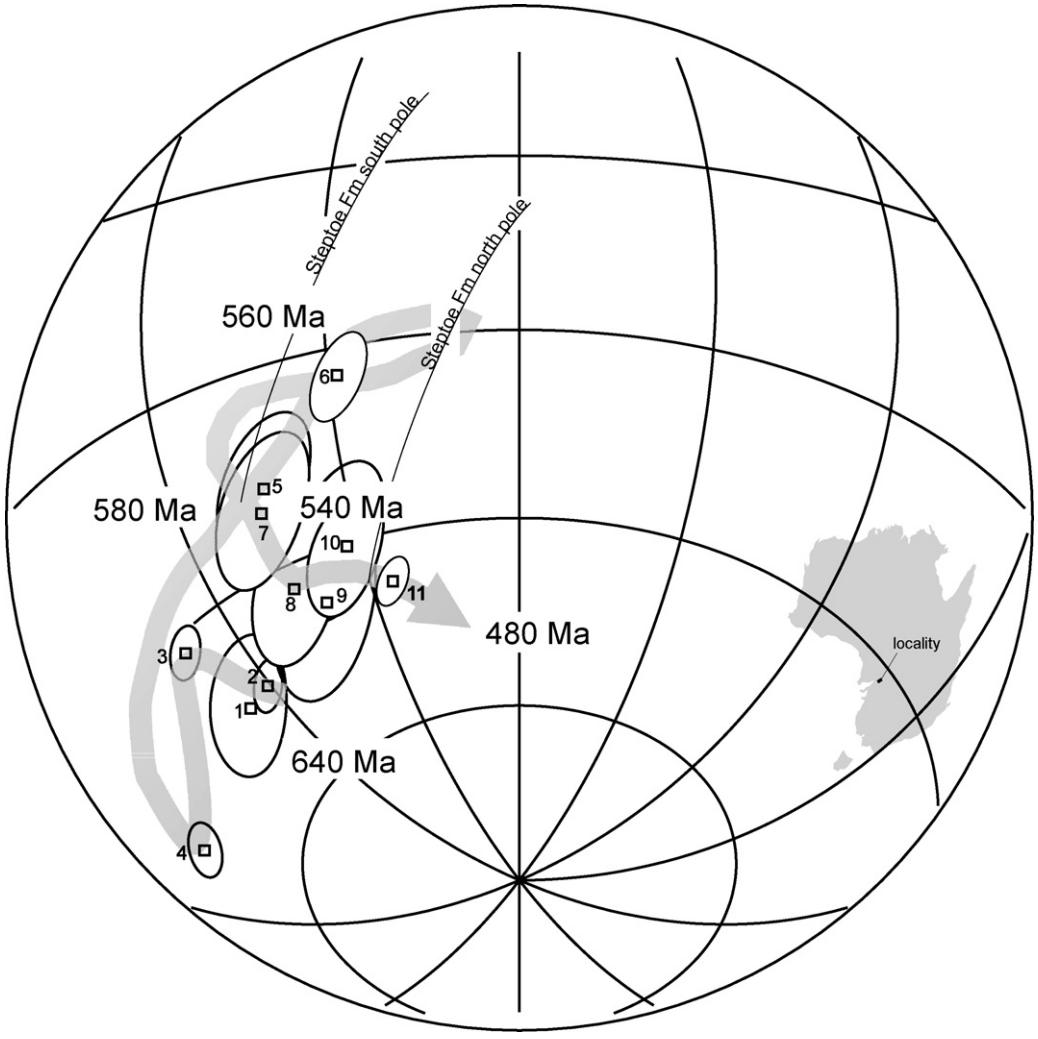

Fig. 10. Updated apparent polar wander path for Neoproterozoic strata of the Adelaide Geosyncline, South Australia, after applying the reliability criteria of Van der Voo (1990). 1, Yaltipena Fm (Sohl et al., 1999); 2–3, Elatina Fm and Nuccaleena Fm, respectively (herein); 4, Brachina Fm (herein); 5, Bunyeroo Fm (Schmidt and Williams, 1996); 6, Wonoka Fm (herein); 7–10, Hawker Group, Billy Creek Fm, Kangaroo Island red beds and Lake Frome Group (basal), respectively (all Klootwijk, 1980); 11, Black Hill Norite (Schmidt et al., 1993) (see Table 7 for reliability criteria).

listed in Table 7 and plotted in Fig. 10. Positive tectonic fold tests at high levels of confidence have been obtained for distinctive ChRM directions from each of the Brachina, Bunyeroo and Wonoka formations. The data form two distinct apparent polar wander paths; one from the late Cryogenian Yaltipena Formation and Elatina Formation through the lower Ediacaran to the Wonoka Formation; the second from the Early Cambrian Hawker Group to the post-Delamerian Black Hill Norite. In Fig. 10 these two trends are joined although no pole positions directly link the two groups.

The systematic pole paths of both these segments lend some confidence to their validity. The steady shift from the Yaltipena pole and nearby Elatina pole, through the Nuccaleena pole and then with a loop through the Brachina pole to the Bunyeroo pole and further away to the Wonoka pole seems to reflect a steady change in both palaeolatitude and azimuthal orientation. The younger, Cambrian path shows a steady decrease of palaeolatitude from the Hawker Group, crossing the equator into the other hemisphere by post-Delamerian (Early Ordovician) times marked by the pole from the post-tectonic Black Hill Norite (487 ± 5 Ma; Schmidt et al., 1993). How the late Ediacaran path links to the Cambrian path is unclear. Attempts to determine high-quality pole positions for the late Ediacaran Bonney Sandstone and Rawnsley Quartzite (Fig. 1) have failed so far (Embleton and Giddings, 1974; McWilliams and McElhinny, 1980). Fig. 10 also shows loci for north and south palaeopole alternatives for the inclination-only data from the Steptoe Formation (Officer Basin; see Fig. 9). When declinations are unavailable, such as for (azimuthally) unoriented drill core, there are alternative loci depending upon the polarity chosen. For low-inclination data the ambiguity is marked and in the case shown in Fig. 10 it is not possible to determine which locus is correct.

7. Conclusions

The results of fold tests for tepee-like structures in the early Ediacaran Nuccaleena Formation, which formed during early diagenesis, suggest that their ChRM was acquired also during early diagenesis. The regional fold test is positive with 99% confidence, demonstrating that the ChRM pre-dates the late Early to Late Cambrian Delamerian Orogeny, consistent with our findings from the tepee-like structures for early remanence acquisition of the Nuccaleena Formation.

Although the acquisition of remanence in the Nuccaleena Formation is early, there is nevertheless some time lag between deposition and magnetisation which may be a significant fraction of the duration of deposition of the entire unit. While correlations over several kilometres may appear sound, we are unable to confidently correlate polarity transitions over hundreds of kilometres. This inability invalidates attempts at intercontinental comparisons of individual polarity transitions within late Neoproterozoic cap carbonates.

By examining both 12 T saturation remanence anisotropy and elongation–inclination systematics (Tauxe and Kent, 2004), we have found no evidence for major compaction-related inclination shallowing in the Elatina Formation. The difference in inclination between late Cryogenian and early Ediacaran strata may well be related to the time gap represented by the disconformity to low-angle unconformity at the sequence boundary between the Elatina and Nuccaleena formations. A minimum peak rate of 16–18 cm year^{-1} for plate motion gives a time interval of less than 5–6 million years. The Cryogenian–Ediacaran inclination difference therefore may be a question not of inclination error but as to how much time the Cryogenian–Ediacaran sequence boundary represents and the rate of coincident polar wander.

We suggest that this time gap between the termination of Elatina deposition and the beginning of Nuccaleena carbonate accumulation may be a significant factor in the enigmatic juxtaposition of glacial deposits and cap carbonates. Such a time gap between deglaciation and cap carbonate deposition conflicts, however, with a basic tenet of the snowball Earth hypothesis that carbonate deposition occurred during rapid deglaciation (Hoffman and Schrag, 2002). Accepting that the Proterozoic geomagnetic field approximated a geocentric axial dipole (McElhinny, 2004; Williams and Schmidt, 2004b), other explanations of pre-Ediacaran glaciation and cold climate near sea-level in low palaeolatitudes also should be considered, for example a “near-snowball” or “slushball” Earth (Allen and Etienne, 2008) and a high obliquity (Williams, 2008). Currently, however, no hypothesis for such glaciation is without its difficulties.

Acknowledgements

We thank Peter Cawood and Rob Woodward (University of Western Australia, Perth), for providing access to palaeomagnetic facilities and the superconducting magnet, respectively. Mark Lackie (Macquarie University, Sydney) kindly allowed the use of the Sapphire susceptibility instrument. CSIRO Exploration and Mining, Sydney, and the Discipline of Geology and Geophysics, University of Adelaide, provided facilities for our work. We thank Dennis Kent, Linda Sohl and Nick Christie-Blick for providing specimen ChRM directions for the Elatina Formation. Thanks are due to Lisa Tauxe, Ken Kodama and Dennis Kent for providing a preprint of their paper, and to Nick Lemon, Vic Gostin, David McKirdy and Wolfgang Preiss for helpful discussions. Critical comments by Mark Lackie, Keith Scott, Dennis Kent and an anonymous reviewer improved the manuscript. The Department of Environment & Heritage of South Australia and the Aboriginal Traditional Owners are thanked for permitting access and sampling in National Parks.

Appendix A. Sampling sites

Site NF01. Ediacaran GSSP site on south bank of Enorama Creek at 31°20′S, 138°38′E (27470 mE 653110 mN Oraparinna 1:50,000 Topographic Sheet 6635-3). Cream buff dolostone tepee-like structure. Regional bedding DDA 318°, dip 23°.

Sites NF02–05. Second Plain, creek exposure at 31°10′S, 138°48′E (Wirrealpa 1:50,000 Topographic Sheet 6635-1). DDA 51°, dip 15°.

Site NF06. North side of Parachilna Gorge, creek exposure at 31°08′S, 138°31′E (Blinman 1:50,000 Topographic Sheet 6635-4). DDA 304°, dip 85°.

Site NF07. Just west of turn-off to Nuccaleena Mine, creek exposure at 31°01′S, 138°33′E (Blinman 1:50,000 Topographic Sheet 6635-4). Tepee-like structures; various attitudes, see text.

Site NF08. Angorichina Creek 500 m south of Angorichina Hostel, at 31°08′S, 138°34′E (Blinman 1:50,000 Topographic Sheet 6635-4). Tepee-like structure; various attitudes, regional attitude DDA 215°, dip 36°.

Site NF09. Tributary of Mount Chambers Creek, at 30°58′S, 138°14′E (Wertaloona 1:50,000 Topographic Sheet 6736-3). DDA 318°, dip 22°.

Site NF10. 200 m north of Big Weepowie crossing of Arkaba Creek, at 31°41′S, 138°35′E (Wilpena 1:50,000 Topographic Sheet 6634-4). DDA 66°, dip 43°.

Site NF11. Warren Gorge, Nuccaleena Formation to Brachina Formation transition, small quarry at 32°11′S, 138°00′E (Willochra 1:50,000 Topographic Sheet 6533-4). DDA 101°, dip 68°.

Site NF12. Buckaringa Gorge, Nuccaleena Formation to Brachina Siltstone transition, road cut at 32°07′S, 138°02′E (Willochra 1:50,000 Topographic Sheet 6533-4). Nuccaleena DDA 114°, dip 48°; transition beds DDA 117°, dip 53°.

References

Allen, J.R.L., 1982. Sedimentary Structures: Their Character and Physical Basis. Vol. I. Developments in Sedimentology 30A. Elsevier, Amsterdam, 593 p.

Allen, P.A., Etienne, J.L., 2008. Sedimentary challenge to Snowball Earth. Nature Geoscience 1, 817–825.

Allen, P.A., Hoffman, P.F., 2005. Extreme winds and waves in the aftermath of a Neoproterozoic glaciation. Nature 433, 123–127.

Ambrose, G.J., 1973. The geology and geochemistry of Adelaidean sediments, Mount Painter Province, South Australia, with emphasis on the Upper Umberatana Group. BSc (Honours) Thesis, University of Adelaide, Australia, 46 p.

Bagnold, R.A., 1965. The Physics of Blown Sand and Desert Dunes. Methuen, London, 265 p.

Biggin, A.J., Strik, G.H.M.A., Langereis, C.G., 2008. Evidence for a very-long-term trend in geomagnetic secular variation. Nature Geoscience 1, 396–398.

Borradaile, G., 1973. Curves for the determination of compaction using deformed cross-bedding. Journal of Sedimentary Petrology 43, 1160.

Coats, R.P., Blissett, A.H., 1971. Regional and economic geology of the Mount Painter Province. Geological Survey of South Australia Bulletin 43, 426 p.

Coats, R.P., Horwitz, R.C., Crawford, A.R., Campana, B., Thatcher, D., 1969. Mount Painter Province 1:125,000 geological sheet. Geological Atlas Special Series, Geological Survey of South Australia, Adelaide.

Coats, R.P., Callen, R.A., Williams, A.F., 1973. Copley 1:250,000 geological sheet, SH 54-9. Geological Survey of South Australia, Adelaide.

Coe, R.S., Glatzmaier, G.A., 2006. Symmetry and stability of the geomagnetic field. Geophysical Research Letters 33, L21311, doi:10.1029/2006GL027903.

Corey, M.A., Simonson, B.M., Loope, D.B., 2005. Physical compaction as a cause of reduced cross-bed dip angle in the Navajo Sandstone. Geological Society of America Abstracts with Programs 37 (7), 254.

Corkeron, M., 2007. 'Cap carbonates' and Neoproterozoic glacigenic succession from the Kimberley region, north-west Australia. Sedimentology 54, 871–903.

Corkeron, M., 2008. Deposition and palaeogeography of a glacigenic Neoproterozoic succession in the east Kimberley, Australia. Sedimentary Geology 204, 61–82.

Drexel, J.F., Preiss, W.V. (Eds.), 1995. The Geology of South Australia, volume 2, The Phanerozoic. Geological Survey of South Australia Bulletin 54, 347 p.

Dunlop, D.J., Yu, Y., 2004. Intensity and polarity of the geomagnetic field during Precambrian time. In: Channell, J.E.T., Kent, D.V., Lowrie, W., Meert, J.G. (Eds.), Timescales of the Paleomagnetic Field. American Geophysical Union Geophysical Monograph 145, pp. 85–100.

Elston, D.P., Enkin, R.J., Baker, J., Kisilevsky, D.K., 2002. Tightening the belt: Paleomagnetic–stratigraphic constraints on deposition, correlation, and deformation of the Middle Proterozoic (ca. 1.4 Ga) Belt–Purcell Supergroup, United States and Canada. Geological Society of America Bulletin 114, pp. 619–638.

Embleton, B.J.J., Giddings, J.W.G., 1974. Late Precambrian and Lower Palaeozoic palaeomagnetic results from South Australia and Western Australia. Earth and Planetary Science Letters 22, 355–365.

Embleton, B.J.J., Williams, G.E., 1986. Low palaeolatitude of deposition for late Precambrian periglacial varvites in South Australia: Implications for palaeoclimatology. Earth and Planetary Science Letters 79, 419–430.

Enkin, R.J., Mahoney, J.B., Baker, J., Riesterer, J., Haskin, M.L., 2003. Deciphering shallow paleomagnetic inclinations. 2. Implications from Late Cretaceous strata overlapping the Insular/Intermontane Superterrane boundary in the southern Canadian Cordillera. Journal of Geophysical Research 108, no. B4, 2186, doi:10.1029/2002JB001983.

Fisher, R., 1953. Dispersion on a sphere. Proceedings of the Royal Society of London A217, 295–305.

Foden, J., Elburg, M.A., Dougherty-Page, J., Burtt, A., 2006. The timing and duration of the Delamerian Orogeny: Correlation with the Ross Orogen and implications for Gondwana assembly. Journal of Geology 114, 189–210.

Font, E., Trindade, R.I.F., Nédélec, A., 2005. Detrital remanent magnetization in haematite-bearing Neoproterozoic Puga cap dolostone. Amazon craton: a rock magnetic and SEM study. Geophysical Journal International 163, 491–500.

Forbes, B.G., Preiss, W.V., 1987. Stratigraphy of the Wilpena Group. In: Preiss, W.V. (Compiler), The Adelaide Geosyncline. Late Proterozoic Stratigraphy, Sedimentation. Palaeontology and Tectonics. Geological Survey of South Australia Bulletin 53, pp. 211–248.

Gallet, Y., Pavlov, V.E., Semikhatov, M.A., Petrov, P.Y., 2000. Late Mesoproterozoic magnetostratigraphic results from Siberia: paleogeographic implications and magnetic field behavior. Journal of Geophysical Research 105, 16481–16499.

Gammon, P.R., McKirdy, D.M., Smith, H.D., 2005. The timing and environment of tepee formation in a Marinoan cap carbonate. Sedimentary Geology 177, 195–208.

Gradstein, F.M., Ogg, J.G., Smith, A.G., 2004. A Geologic Time Scale. Cambridge University Press, Cambridge, 589 p.

Gee, J.S., Kent, D.V., 2007. Source of oceanic magnetic anomalies and the geomagnetic polarity time scale. In: Kono, M. (Ed.), Treatise on Geophysics, Volume 5. Geomagnetism. Elsevier, Amsterdam, pp. 455–507.

Grey, K., Hocking, R.M., Stevens, M.K., Bagas, L., Carlsen, G.M., Irimies, F., Pirajno, F., Haines, P.W., Apak, S.N., 2005. Lithostratigraphic nomenclature of the Officer Basin and correlative parts of the Paterson Orogen, Western Australia. Geological Survey of Western Australia Report 93, 89 pp. Available at http://www.doir.wa.gov.au/GSWA/onlinepublications.

Halls, H.C., 1991. The Matachewan dyke swarm, Canada: An early Proterozoic magnetic field reversal. Earth and Planetary Science Letters 105, 279–292.

Hoffman, P.F., Schrag, D.P., 2002. The snowball Earth hypothesis: testing the limits of global change. Terra Nova 14, 129–155.

Hoffman, P.F., Halverson, G.P., Domack, E.W., Husson, J.M., Higgins, J.A., Schrag, D.P., 2007. Are basal Ediacaran (635 Ma) post-glacial "cap dolostones" diachronous? Earth and Planetary Science Letters 258, 114–131.

Jackson, M.J., Banerjee, S.K., Marvi, J.A., Lu, R., Gruber, W., 1991. Detrital remanence, inclination errors, and anhysteretic remanence anisotropy: quantitative model and experimental results. Geophysical Journal International 104, 95–103.

Jelinek, V., 1981. Characterization of magnetic fabric of rocks. Tectonophysics 79, 63–67.

Jenkins, G.S., McMenamin, M.A.S., McKay, C.P., Sohl, L. (Eds.), 2004. The Extreme Proterozoic: Geology, Geochemistry and Climate. American Geophysical Union Geophysical Monograph 146, 229 p.

Jiang, G., Kennedy, M.J., Christie-Blick, N., Wu, H., Zhang, S., 2006. Stratigraphy, sedimentary structures, and textures of the late Neoproterozoic Doushantuo cap carbonate in south China. Journal of Sedimentary Research 76, 978–995.

Kendall, C.G., St, C., Warren, J., 1987. A review of the origin and setting of tepees and their associated fabrics. Sedimentology 34, 1007–1027.

Kennedy, M.J., 1996. Stratigraphy, sedimentology, and isotopic geochemistry of Australian Neoproterozoic postglacial cap dolostones: deglaciation, $\delta^{13}C$ excursions, and carbonate precipitation. Journal of Sedimentary Research 66, 1050–1064.

Kent, J.T., Briden, J.C., Mardia, K.V., 1983. Linear and planar structure in ordered multivariate data as applied to progressive demagnetization of palaeomagnetic remanence. Geophysical Journal of the Royal Astronomical Society 75, 593–621.

Kilner, B., Mac Niocaill, C., Brasier, M., 2005. Low-latitude glaciation in the Neoproterozoic of Oman. Geology 33, 413–416.

King, R.F., 1955. The remanent magnetism of artificially deposited sediments. Monthly Notices of the Royal Astronomical Society. Geophysical Supplement 7, 115–134.

Klootwijk, C.T., 1980. Early Palaeozoic palaeomagnetism in Australia. Tectonophysics 64, 249–332.

Knoll, A.H., Walter, M.R., Narbonne, G.M., Christie-Blick, N., 2004. A new period for the geologic time scale. Science 305, 621–622.

Knoll, A.H., Walter, M.R., Narbonne, G.M., Christie-Blick, N., 2006. The Ediacaran Period: a new addition to the geologic time scale. Lethaia 39, 13–30.

Kodama, K.P., Dekkers, M.J., 2004. Magnetic anisotropy as an aid to identifying CRM and DRM in red sedimentary rocks. Studies in Geophysics and Geodesy 48, 747–766.

Lavin, C., 1992. The origin of Proterozoic, post-glacial dolomites – the Nuccaleena Formation. BSc (Honours) Thesis, University of Melbourne, Australia, 63 p.

Lemon, N.M., Gostin, V.A., 1990. Glacigenic sediments of the late Proterozoic Elatina Formation and equivalents, Adelaide Geosyncline, South Australia. In: Jago, J.B., Moore, P.S. (Eds.), The Evolution of a Late Precambrian–Early Palaeozoic Rift Complex: The Adelaide Geosyncline. Geological Society of Australia Special Publication 16, pp. 149–163.

Li, Z.X., 2000. New palaeomagnetic results from the 'cap dolomite' of the Neoproterozoic Walsh Tillite, northwestern Australia. Precambrian Research 100, 359–370.

Li, Z.X., Powell, C.Mc.A., 1993. Magnetic fabric in the mid-Cambrian rocks of the Central Flinders Zone and implications for the regional tectonic history. Tectonophysics 223, 165–176.

McElhinny, M., 2004. Geocentric axial dipole hypothesis: a least squares perspective. In: Channell, J.E.T., Kent, D.V., Lowrie, W., Meert, J.G. (Eds.), Timescales of the Paleomagnetic Field. American Geophysical Union Geophysical Monograph 145, pp. 1–12.

McFadden, P.L., 1990. A new fold test for palaeomagnetic studies. Geophysical Journal International 103, 163–169.

McFadden, P.L., Lowes, F.J., 1981. The discrimination of mean directions drawn from Fisher distributions. Geophysical Journal of the Royal Astronomical Society 67, 19–33.

McFadden, P.L., McElhinny, M.W., 1990. Classification of the reversal test in palaeomagnetism. Geophysical Journal of the Royal Astronomical Society 103, 725–729.

McWilliams, M.O., 1977. Late Precambrian palaeomagnetism of Australia and Africa. Ph.D. Thesis, Australian National University, Canberra, Australia, 162 p.

McWilliams, M.O., McElhinny, M.W., 1980. Late Precambrian paleomagnetism of Australia: the Adelaide Geosyncline. Journal of Geology 88, 1–26.

Meert, J.G., Van der Voo, R., 1994. The Neoproterozoic (1000-540 Ma) glacial intervals: no more snowball earth? Earth and Planetary Science Letters 123, 1–13.

Meert, J.G., Van der Voo, R., Powell, C.Mc.A., Li, Z.-X., McElhinny, M.W., Chen, Z., Symons, D.T.A., 1993. A plate-tectonic speed limit? Nature 363, 216–217.

Pisarevsky, S.A., Li, Z.X., Grey, K., Stevens, M.K., 2001. A palaeomagnetic study of Empress 1A, a stratigraphic drillhole in the Officer Basin: evidence for a low-latitude position of Australia in the Neoproterozoic. Precambrian Research 110, 93–108.

Pisarevsky, S.A., Wingate, M.T.D., Stevens, M.K., Haines, P.W., 2007. Palaeomagnetic results from the Lancer 1 stratigraphic drillhole, Officer Basin, Western Australia, and implications for Rodinia reconstructions. Australian Journal of Earth Sciences 54, 561–572.

Plummer, P.S., 1978. Note on the palaeoenvironmental significance of the Nuccaleena Formation (upper Precambrian), central Flinders Ranges, South Australia. Journal of the Geological Society of Australia 25, 395–402.

Preiss, W.V., 1993. Neoproterozoic. In: Drexel, J.F., Preiss, W.V., Parker, A.J. (Eds.), The Geology of South Australia, volume 1, The Precambrian. Geological Survey of South Australia Bulletin 54, pp. 171–203.

Preiss, W.V., 2000. The Adelaide Geosyncline of South Australia and its significance in Neoproterozoic continental reconstruction. Precambrian Research 100, 21–63.

Preiss, W.V., Dyson, I.A., Reid, P.W., Cowley, W.M., 1998. Revision of lithostratigraphic classification of the Umberatana Group. MESA Journal 9, 36–42.

Raub, T.D., Evans, D.A.D., 2005. High-resolution magnetostratigraphy of Australia's Marinoan cap carbonates. Supercontinents and Earth Evolution Symposium, Perth, Western Australia, September 2005, Abstracts, p. 53.
Raub, T.D., Evans, D.A., 2006. Magnetic reversals in basal Ediacaran cap carbonates: A critical review. Eos, Transactions of the American Geophysical Union 87 (36), Joint Assembly Supplement, Abstract GP41B-02.
Raub, T.D., Evans, D.A.D., 2008. Paleolatitudes of Neoproterozoic snowball glacial deposits: Biases and synthesis. 33rd International Geological Congress, Oslo, August 2008, Abstract CGC-04.
Raub, T.D., Evans, D.A.D., Smirnov, A.V., 2007. Siliclastic prelude to Elatina Nuccaleena deglaciation: lithostratigraphy and rock magnetism of the base of the Ediacaran system. Geological Society of London Special Publication 286, 53–76.
Rittenhouse, G., 1972. Cross-bedding dip as a measure of sandstone compaction. Journal of Sedimentary Petrology 42, 682–683.
Roberts, N., Piper, J.D.A., 1989. A description of the behaviour of the Earth's magnetic field. In: Jacobs, J.A. (Ed.), Geomagnetism. Elsevier, New York, pp. 163–260.
Schmidt, P.W., Williams, G.E., 1995. The Neoproterozoic climatic paradox: Equatorial palaeolatitude for Marinoan glaciation near sea level in South Australia. Earth and Planetary Science Letters 134, 107–124.
Schmidt, P.W., Williams, G.E., 1996. Palaeomagnetism of the ejecta-bearing Bunyeroo Formation, late Neoproterozoic, Adelaide fold belt, and the age of the Acraman impact. Earth and Planetary Science Letters 144, 347–357.
Schmidt, P.W., Clark, D.A., Rajagopolan, S., 1993. An historical perspective of the Early Palaeozoic APWP of Gondwana: New results from the Early Ordovician Black Hill Norite, South Australia. Exploration Geophysics 24, 257–262.
Schmidt, P.W., Williams, G.E., Embleton, B.J.J., 1991. Low palaeolatitude of Late Proterozoic glaciation: early timing of remanence in haematite of the Elatina Formation, South Australia. Earth and Planetary Science Letters 105, 355–367.
Sohl, L.E., Christie-Blick, N., Kent, D.V., 1999. Paleomagnetic polarity reversals in Marinoan (ca. 600 Ma) glacial deposits of Australia: Implications for the duration of low-latitude glaciation in Neoproterozoic time. Geological Society of America Bulletin 111, 1120–1139.
Strik, G.T.S., Blake, T.S., Zegers, T.E., White, S.H., Langereis, C.G., 2003. Palaeomagnetism of flood basalts in the Pilbara Craton, Western Australia: Late Archaean continental drift and the oldest reversal of the geomagnetic field. Geophysical Journal of Research 108, 2551, doi:10.1029/2003JB002475.
Tauxe, L., Kent, D.V., 2004. A simplified statistical model for the geomagnetic field and the detection of shallow bias in palaeomagnetic inclinations: Was the ancient magnetic field dipolar? In: Channell, J.E.T, Kent, D.V., Lowrie, W., Meert, J.G. (Eds.), Timescales of the Paleomagnetic Field. American Geophysical Union Geophysical Monograph 145, pp. 101–115.
Tauxe, L., Kodama, K.P., Kent, D.V., 2008. Testing corrections for paleomagnetic inclination error in sedimentary rocks: a comparative approach. Physics of the Earth and Planetary Interiors 169, 152–165, doi:10.1016/j.pepi.2008.05.006.
Trindade, R.I.F., Macouin, M., 2007. Palaeolatitude of glacial deposits and palaeogeography of Neoproterozoic ice ages. C. R. Geoscience 339, 200–211.
Trindade, R.I.F., Font, E., D'Agrella-Filho, M.S., Nogueira, A.C.R., Riccomini, C., 2003. Low-latitude and multiple geomagnetic reversals in the Neoproterozoic Puga cap carbonate, Amazon craton. Terra Nova 15, 433–440.
Turner, P., 1980. Continental Red Beds. Developments in Sedimentology 29, Elsevier, Amsterdam, 562 p.
Van der Voo, R., 1990. The reliability of paleomagnetic data. Tectonophysics 184, 1–9.
Williams, G.E., 1979. Sedimentology, stable-isotope geochemistry and palaeoenvironment of dolostones capping late Precambrian glacial sequences in Australia. Journal of the Geological Society of Australia 26, 377–386.
Williams, G.E., 1991. Upper Proterozoic tidal rhythmites, South Australia: sedimentary features, deposition, and implications for the earth's paleorotation. In: Smith, D.G., Reinson, G.E., Zaitlin, B.A., Rahmani, R.A. (Eds.), Clastic Tidal Sedimentology. Canadian Society of Petroleum Geologists Memoir 16, pp. 161–178.
Williams, G.E., 1996. Soft-sediment deformation structures from the Marinoan glacial succession. Adelaide foldbelt: implications for the palaeolatitude of late Neoproterozoic glaciation. Sedimentary Geology 106, 165–175.
Williams, G.E., 2000. Geological constraints on the Precambrian history of Earth's rotation and the Moon's orbit. Reviews of Geophysics 38, 37–59.
Williams, G.E., 2008. Proterozoic (pre-Ediacaran) glaciation and the high obliquity, low-latitude ice, strong seasonality (HOLIST) hypothesis: principles and tests. Earth-Science Reviews 87, 61–93.
Williams, G.E., Schmidt, P.W., 2004a. Paleomagnetism of the 1.88-Ga Sokoman Formation in the Schefferville–Knob Lake area, Québec, Canada, and implications for the genesis of iron oxide deposits in the central New Québec Orogen. Precambrian Research 128, 167–188.
Williams, G.E., Schmidt, P.W., 2004b. Neoproterozoic glaciation: reconciling low paleolatitudes and the geologic record. In: Jenkins, G.S., McMenamin, M., Sohl, L.E., McKay, C.P. (Eds.), The Extreme Proterozoic: Geology, Geochemistry and Climate. American Geophysical Union Geophysical Monograph 146, pp. 145–159.
Williams, G.E., Schmidt, P.W., Embleton, B.J.J., 1995. Comment on 'The Neoproterozoic (1000-540 Ma) glacial intervals: No more snowball earth?' by Joseph G. Meert and Rob van der Voo. Earth and Planetary Science Letters 131, 115–122.
Williams, G.E., Gostin, V.A., McKirdy, D.M., Preiss, W.V., 2008. The Elatina glaciation, late Cryogenian (Marinoan Epoch), South Australia: sedimentary facies and palaeoenvironments. Precambrian Research 163, 307–331.
Williams, G.E, Gostin, V.A., McKirdy, D.M., Preiss, W.V., Schmidt, P.W., in press. The Elatina glaciation (late Cryogenian), South Australia. In: Neoproterozoic Ice Ages, Geological Society of London Memoir.
Zhang, S., Jiang, G., Han, Y., 2008. The age of the Nantuo Formation and Nantuo glaciation in South China. Terra Nova 20, 289–294.